Ground motion simulations of a major historical earthquake (1660) in the French Pyrenees using recent moderate size earthquakes

Laëtitia Honoré (1), Françoise Courboulex (1) and Annie Souriau (2)

(1) Université de Nice Sophia-Antipolis, INSU-CNRS, Observatoire de la Côte d'Azur, Géoazur, Valbonne, France

(2) CNRS, Université Paul Sabatier, Observatoire Midi-Pyrénées, Toulouse, France

Abbreviated title: Simulation of an historical earthquake in the Pyrenees

Corresponding author:

Laëtitia Honoré

Address: GéoAzur, 250 rue Albert Einstein, 06560, Valbonne, France

Phone: +33(0)492942606

Fax: +33(0)492942610

e-mail: honorel@geoazur.unice.fr

SUMMARY

In regions where only small to moderate size events have been recorded, it is important to be able to simulate in a large frequency band the seismogram of a major earthquake. Using the very good records of a small earthquake (November 15th 2007, M_w=3.6) that occurred in the central French Pyrenees, we simulated the ground motions generated by a magnitude 6.1 earthquake, equivalent to the historical event that stroke the region in 1660. This major earthquake caused many damages and reached a maximum macroseismic intensity of IX on MSK scale. We first validated the simulation method by reproducing the records of the November 17th 2006 earthquake (M_w=4.5) using the 2007 earthquake (M_w=3.6) as empirical Green's function (EGF) to account for path and site effects. A careful analysis of corner frequencies f_c and spectral ratios revealed a clear directivity effect of the rupture process for the largest event. To take into account this effect, we proposed the introduction of a new input parameter in the simulation method. We obtained a very good reproduction of ground motion parameters for all the stations. We then used the records of the 2007 earthquake (M_w=3.6) as an EGF to compute at 11 stations a large number of synthetic accelerograms that aims to account for the possible source variability of an M_w=6.1 earthquake, equivalent to the 1660 historical event. Lastly, we compared our simulation results with intensity data of the 1660 event by using three different Ground Motion Intensity Conversion Equations (GMICEs). We observed that intensity levels predicted by empirical relationships from ground motion simulations were always lower than the macroseismic intensities of the 1660 historical earthquake. To explain this difference, the hypothesis of a possible underestimation of the 1660 event's magnitude is discussed.

Key words: Earthquake ground motions; Earthquake source observations; Site effects; Seismicity and tectonics; Europe.

1. INTRODUCTION

The Pyrenean range is characterized by a moderate seismic activity. Since the systematic deployment of seismic networks, in the early sixties, the largest recorded event reached only a magnitude *Ml*=5.5 (1967/08/13 Arette earthquake, Gagnepain *et al.* 1980). Nonetheless, according to historical catalogues several strong earthquakes with epicentral intensity larger than VIII have been reported (Lambert & Levret-Albaret 1996). One of the most destructive Pyrenean earthquakes occurred in the Central French Pyrenees, on June 21st 1660. Based on accounts of felt shaking and damage levels reported on historical documents, the suspected epicentral region is located a few kilometers south of the pilgrimage city of Lourdes and its magnitude is estimated to be equivalent to 6.1 (Levret *et al.* 1996). With an epicentral intensity assessed to VIII-IX on MSK scale (1964) (SisFrance, BRGM *et al.* 2004), this major historical earthquake induced strong damages in the cities of Lourdes and Bagnères-de-Bigorre.

If such an earthquake were to occur today, it would be likely to produce more destruction and casualties because of build-up area development and increasing population density in the region. Thus, it is of utmost importance to have a thorough knowledge of historical seismicity in order to bring further information for seismic hazard assessment of the region. Pre-instrumental historical events can only be quantified with macroseismic intensities assessed from interpretation of available historical documents. However, to better anticipate a hypothetic future large earthquake by providing information of engineering interest, there is a need for a quantification of ground motions generated by large historical events.

There are mainly three kinds of approaches to estimate the ground motions generated by an earthquake:

(1) Empirical ground motion prediction equations (GMPEs). These equations provide ground motion parameters as a function of magnitude, source-to-site distance and other variables such as local soil conditions or style-of-faulting (e.g.: Reiter 1990; Douglas 2003). These relations are empirically derived through regression analysis of ground motion database. To establish GMPEs one needs data in a large range of magnitude and source-to-site distance. In regions of low to moderate seismicity there are not enough ground motion records to develop a specific GMPE. So, data recorded in other regions of the world have to be used, assuming that they are appropriate for the area under study. GMPEs are essential for seismic

hazard assessment, nevertheless they are neither able to provide accelerograms nor to reproduce specific attenuation conditions and site effects.

(2) Numerical methods. They are based on modelling of both source process and seismic wave propagation in a heterogeneous medium. These methods are promising; however, they are often limited to rather low frequencies due to a poor knowledge of underground velocity medium.

(3) Semi-empirical approaches. They are often based on empirical Green's function (EGF) principle (Hartzell 1978). The idea is to consider records of a small earthquake, located near an event of interest, as reasonable approximation of the impulse response of the medium. Thus, this approach allows simulating seismograms of a large earthquake that account for wave-propagation and site-effects, under assumption of linear soil response.

The goal of this study was to produce ground motion simulations of a magnitude M_w=6.1 earthquake, equivalent to the 1660 historical event, from instrumental data of recent small to moderate Pyrenean earthquakes. To do so, we propose to use the method developed by Kohrs-Sansorny *et al.* (2005), where ground motion simulations of a large earthquake are generated by using a stochastic summation of one small earthquake records regarded as empirical Green's functions. This method is easy to apply and has the advantage of requiring very few input parameters.

On November 17th 2006 and November 15th 2007, the occurrences of two Pyrenean earthquakes (respectively M_w=4.5 and M_w=3.6) in the suspected epicentral area of the 1660 historical event, well recorded by a large number of accelerometric stations (French Permanent Accelerometric Network, Pequegnat *et al*. 2008) provide us with the opportunity to implement an EGF simulation method.

In a first step, we propose to use the 2007 earthquake (M_w=3.6) as an empirical Green's function in order to reproduce ground motions generated by the 2006 earthquake (M_w=4.5). The direct comparison between simulation results and ground motions observed during the 2006 earthquake will allow us to test the efficiency of the method.

In a second step, we aim to generate ground motion simulations of a magnitude M_w=6.1 earthquake, by using the 2007 earthquake (M_w=3.6) as an empirical Green's function. These simulations will provide us with estimation of ground motions that could realistically be generated at specific Pyrenean stations by an earthquake equivalent to the 1660 historical event. In order to compare our simulation results with intensity data of the 1660 event, empirical relationships between instrumental ground motion parameters and macroseismic intensities (GMICEs) will be used (Fig. 1).

2. SEISMOTECTONIC CONTEXT

2.1. Tectonic setting and seismicity

The Pyrenean range results from the North-South convergence between the Eurasian plate and the Iberian microplate, initiated 65 my ago after a rifting episode which opened a narrow rift between the two plates (Choukroune 1992, and Olivet 1996, for reviews). The boundary between the two plates, the North Pyrenean fault, runs all along the range and is clearly identified thanks to the important related Moho jump (Hirn *et al.* 1980; Gallart *et al.* 1981). The present differential motion between the two plates is small, less than one mm/yr (Nocquet & Calais 2004), and recent focal mechanisms in the central part of the range argue in favour of a weak N-S extension (Sylvander *et al.* 2008). In agreement with this low deformation rate, the Pyrenean range is characterized by a moderate seismic activity. The seismicity is monitored by about 40 velocimeters and 30 accelerometers deployed on both the French and Spanish sides. About 600 to 800 events with $Ml > 1$ are located each year all along the range (Fig. 2), but there is in a mean only one or two event with $Ml \geq 5$ each ten years (Souriau & Pauchet 1998; Souriau *et al.* 2001). Most of the focal depths are in the range 4-12 km. The seismicity reveals a general E-W distribution, but with complex fault systems (Gagnepain-Beyneix *et al.* 1982; Souriau *et al.* 2001; Rigo *et al.* 1997; Rigo *et al.* 2005; Ruiz *et al.* 2006).

Although the instrumental seismicity reveals only small to moderate earthquakes, the historical seismicity shows that the Pyrenees have been affected by strong earthquakes (Vogt 1979; Lambert & Levret-Albaret 1996). The period covered by the instrumental seismicity is short compared with the recurrence period of large earthquakes, which must be in the order of centuries (Souriau & Pauchet 1998; Alasset & Meghraoui 2005), so that the instrumental seismicity gives an incomplete image of seismic hazard. For example, the strongest earthquake recorded in Eastern Pyrenees is a Ml=5.3 event (St-Paul-de-Fenouillet in 1996, Rigo *et al.* 1997), which induced only minor damages, whereas the strongest reported historical event (North Catalonia, in 1428) has an estimated magnitude of 6.4-6.5 (Lambert & Levret-Albaret 1996), and killed about 700 people. Historical seismicity is thus of major importance to bring further information for seismic hazard assessment.

Historical events are quantified with macroseismic intensities assessed from felt shaking and damage descriptions reported on historical documents. They allow us to produce maps of macroseismic intensities, to draw isoseist contour lines and in a last step to retrieve

the epicentral region. Finally, by comparing the macroseismic maps of historical and instrumental events, it is possible to ascribe an equivalent magnitude to historical events (Levret *et al.* 1994). This magnitude may however be biased by numerous factors, as the poor knowledge of the focal depth, the regional variations of attenuation, and different focal mechanisms.

The French historical seismicity is well documented back to the 14th century, with about 25 events of maximum intensity larger than VII since the beginning of the 17th century (Lambert & Levret-Albaret 1996). In Fig. 2 are reported the main historical events in the Pyrenees, with their maximal intensity in MSK scale (Medvedev *et al.* 1964). Alike the instrumental seismicity, historical events are distributed all along the range. On the French side, the most important event occurred near Lourdes in 1660, with maximum MSK intensity IX. If a similar event would occur today, it would likely be a major catastrophe. For this reason, we will now focus on this particular event.

2.2. The 1660 historical earthquake

On June 21st, 1660 a major earthquake occurred in the Central French Pyrenees. It is particularly well documented, because there were populated areas in a wide region all around the epicenter. Moreover, it occurred just after the wedding of King Louis XIV in Saint-Jean-de-Luz in Western Pyrenees (Bernard *et al.* 1997). It is one of the most destructive Pyrenean earthquakes. Indeed, from interpretation of available historical documents, it has been felt in a large part of France, up to 500 kilometers away from the epicenter. Part of the cities of Lourdes and Bagnères-de-Bigorre were destroyed, and about 30 deaths are reported. Its epicentral MSK intensity is assessed to VIII-IX and the suspected epicentral region is located about 17 km SE of Lourdes and 13 km SW of Bagnères-de-Bigorre (Figs 2 and 3). The macroseismic epicentral location (42°58'N latitude and 0°04'E longitude) provided by the SisFrance catalogue (BRGM *et al.* 2004) is given with a reliability index "B", corresponding to a location uncertainty of about 10 km. It means that the epicentral location is rather reliable in an area of maximum intensity relatively well circumscribed by an isoseist. Finally, its magnitude is estimated to be equivalent to Ml=6.1±0.4 (Levret *et al.* 1996) using empirical relationships established for the French earthquakes (Levret *et al.* 1994). Cara *et al.* (2008) applied a differential macroseismic method based on the comparison at large epicentral distances between intensities of historical and recent instrumental earthquakes in order to

estimate the moment magnitude M_w of some historical earthquakes in the French Pyrenees. To compute the moment magnitude of the 1660 event, they choose as reference the November 2006 Argelès earthquake and found a magnitude M_w=6.1±0.2. We thus took this magnitude value for our simulations. Uncertainties on the magnitude determination will be discussed at the end of this paper.

3. AN EMPIRICAL GREEN'S FUNCTION SIMULATION METHOD

We aim to simulate a set of realistic accelerograms that could be generated by an earthquake of magnitude 6.1, equivalent to the 1660 historical event, at the same place and with the same focal mechanism than recent recorded events. In order to be able to reproduce propagation and site effects in a large frequency band, we used an empirical Green's function (EGF) approach based on a summation of records of small earthquakes. Among the possible EGF methods**,** we choose the stochastic method in two steps proposed by Kohrs-Sansorny *et al.* (2005) because it requires few input parameters, which is a great advantage for simulating an unknown event. This method is based on the previous works of Joyner & Boore (1986), Wennerberg (1990) and Ordaz *et al.* (1995). It has proved its efficiency for simulating the ground motions of moderate size earthquakes, at the condition that a proper small event is chosen as EGF (Courboulex *et al.* 2010). It has also been recently used to simulate the effects of a rather large earthquake (M_w=6.3) in the south east of France (Salichon *et al.* 2010).

As it is completely described in the paper of Kohrs-Sansorny *et al.* (2005), we only propose here a short presentation of the method. The principle is simple: A large number *k* of time histories called Equivalent Source Time Functions (ESTFs) is generated. Each ESTF, representative to a given rupture process, is then convolved with the small event records *egf(t)* to provide the synthetic signals *S(t)* (Eq. 1).

$$S_k(t) = ESTF_k(t) * egf(t) \quad (1)$$

The ESTFs are built using a random process based on probability densities proposed by Ordaz *et al.* (1995), which ensure an average reproduction of the ω^{-2} model (Aki 1967*;* Brune 1970) for all frequencies. N^4 points are chosen over the whole source duration T_c. The ESTFs

generated by the random process are different one from the other, and they can indirectly account for different types of ruptures and produce a large variability in the ground motion. Because we do not want to impose a constant stress drop for the small and the target event, the common scaling relation $Mo \propto F_c^{-3}$ (Brune 1970; Kanamori & Anderson 1975) becomes $Mo \propto \Delta\Sigma \, . F_c^{-3}$ (Beeler *et al.* 2003; Kanamori & Rivera 2004), where $\Delta\Sigma$ is the stress drop and F_c the corner frequency. We define the parameter C as the stress drop ratio between the large and the small earthquake, and N as the ratio between the corner frequency of the small event f_c and that of the large event F_c. In practice N will be set integer, which implies that only discrete values of F_c and C will be possible.

One interest of this method is that the number of input parameters is reduced. Indeed, the only parameters that have to be specified are: (1) The seismic moment (m_0) and the corner frequency (f_c) of the small event taken as EGF, which are directly determined from the data; (2) The seismic moment (M_0) of the target event; (3) The ratio C between the static stress-drop of the target event ($\Delta\Sigma$) and that of the small event ($\Delta\sigma$). These parameters are linked by the relationships (Eq. 2):

$$CN^3 = \frac{M_0}{m_0} \quad \text{where} \quad N = \left| \frac{f_c}{F_c} \right|, \quad C = \frac{\Delta\Sigma}{\Delta\sigma} \quad \text{and} \quad T_c = 1/F_c \qquad (2)$$

4. DATA

4.1. Data selection and network

In the present study, instrumental data of two recent Pyrenean earthquakes are used: the November 17th, 2006 earthquake (Ml=5.0) called Argelès earthquake (Sylvander *et al.* 2008) and the November 15th, 2007 earthquake (Ml=4.1). These two events occurred at one year interval almost at the same location. From the parameters of these earthquakes (Table 1), we infer a great similarity between the two events. The distance between the two epicentres is less than one kilometre and the difference in depth is about two kilometres. These earthquakes are located a few kilometres south to the North Pyrenean Fault and occurred on an East-West

oriented normal fault. This tectonic structure, previously identified by Rigo *et al.* (2005), is suspected to be responsible for the 1660 historical earthquake, assuming a normal fault mechanism. Beside their interest to have occurred in the suspected epicentral region of the 1660 historical earthquake, these earthquakes were selected because they satisfy all requirements to be used as empirical Green's functions in our simulation method. Both earthquakes have similar normal fault focal mechanisms and occurred at almost the same location. Moreover, these earthquakes were recorded with a good signal-to-noise ratio by a large number of accelerometric stations, belonging to the French Permanent Accelerometric Network (Pequegnat *et al*. 2008). For this study we selected 11 accelerometric stations with epicentral distances lower than 100 km. These stations are maintained by the Observatoire Midi-Pyrénées in Toulouse (OMP) and the Bureau de Recherche Géologiques et Minières (BRGM). The local site geology for these stations is based on superficial geological considerations, with a simplified soil classification into two categories: rock sites and sedimentary sites (see: http://www-rap.obs.ujf-grenoble.fr) (Table 2; Fig. 4).

4.2. Data analysis for determination of input parameters

The simulation method used in this study is based on the knowledge of a few input parameters which can be determined from data analysis of the two selected earthquakes. The parameters we need are seismic moment, corner frequency and static stress drop ratio.

4.2.1. Seismic moment

For the 2006 earthquake, we took the seismic moment determined by Sylvander *et al.* (2008): $M_0 = 5.32 \times 10^{15} (N.m)$, corresponding to a moment magnitude $M_w = 4.48$. In order to determine the seismic moment of the 2007 earthquake, we used a spectral ratio analysis between the recordings of the 2006 (Ml=5.0) and the 2007 (Ml=4.1) earthquakes. We obtained a moment of $m_0 = 2.38 \times 10^{14} (N.m)$ for the 2007 earthquake, which corresponds to a moment magnitude $m_w = 3.58$. As already observed by Drouet *et al.* (2005) for Pyrenean earthquakes in this range of magnitudes, moment magnitudes M_w are about 0.5 units smaller than local magnitudes Ml.

4.2.2. Corner frequency

Assuming a Brune's ω^{-2} source model (Brune 1970), the corner frequencies of the 2006 and 2007 earthquakes are determined from displacement spectra analysis. On Fourier displacement spectra, we fit at high frequency a ω^{-2} slop line and at low frequency a ω^{0} slop line: the intersection between these two asymptotes gives the corner frequency. For the 2007 earthquake (M_w=3.6), the value of the corner frequency is almost the same at all the stations and can be averaged over all the values determined from available records (f_c = 3.3 Hz ± 0.3 Hz). However, for the 2006 earthquake (M_w=4.5), corner frequency values appear to be clearly dependant on the azimuth of the station (Fig. 5). This variability can be due to a directivity effect of the rupture process.

4.3. Directivity effect of the M_w=4.5 earthquake

During data analysis of the 2006 earthquake (M_w=4.5), we found that corner frequency values obtained at each station vary with event-to-station angle. This result is confirmed by using spectral ratios between the 2006 (M_w=4.5) and the 2007 (M_w=3.6) earthquakes. This analysis has the advantage of theoretically eliminating path and site effects that could affect source parameters determination.

If we consider that corner frequency F_c enables to estimate rupture duration T_r by using the approximation $T_r = 1/F_c$, we obtain rupture durations having also an azimutal dependence, which may be interpreted as a directivity effect of the rupture process. Then, rupture duration and corner frequency values obtained at a given station are in fact apparent rupture duration T_a and apparent corner frequency F_a. Assuming a simple line source model with unilateral constant rupture propagation, the apparent duration of the source T_a seen at a given station can be expressed as following (Eq. 3):

$$T_a = T_r - \frac{T_r \times V_r}{c} \cos\left(\theta - \theta_0\right) \qquad (3)$$

where θ and θ_0 are the azimuth of the station and the rupture propagation respectively, V_r is rupture velocity, c is wave velocity around the source and T_r is actual source duration. For a directive station (θ-θ_0=0°), the apparent rupture duration is shorter than for an anti-directive

station (θ-θ_0=180°) and it results in larger ground motion amplitudes for a directive station than for an anti-directive station.

We consider that the apparent duration T_a of the source time function at a given station is given by $T_a = 1/F_a$. For unilateral rupture propagation, the duration T_a of the apparent source time function at a given station can be written in a linear form (Eq. 4):

$$T_a = T_r - \Gamma \Delta \quad (4)$$

where T_r represents the real duration of the source process, Δ the horizontal length of the rupture and Γ the directivity factor, defined as (Eq. 5):

$$\Gamma = cos\ (\theta - \theta_0)/c \quad (5)$$

We systematically investigated each azimuth θ_0 in order to find the value that gives the best linear correlation coefficient. We obtain a very good correlation coefficient of 0.97 for a direction of the rupture propagation of N114° (Fig. 6). This result is in good accordance with the focal mechanism and the azimuth of the main faults in the region. With this value of θ_0, T_a values are plotted on Fig. 6 as a function of Γ. From this figure we obtain the duration of the rupture process: T_a is equal to 0.81 seconds for Γ=0. This value is realistic for such an earthquake.

In order to try to infer the rupture velocity and the source dimension, the value of c has to be defined. Because we determined the F_c value from both P and S waves, we take in consideration both wave velocities. We took a Vs value of 3.5 km/sec in the source region as proposed by Drouet *et al.* (2005) and a V_P/V_S ratio of 1.7. In each case we obtain a very low rupture velocity from 1.3 to 1.8 km/sec. It gives a maximum horizontal length of the rupture of 1.4 km.

Finally, stations can be classified into two main groups: directive stations in the rupture direction to the East (PYAS, PYBB, PYLI, PYLU,) and anti-directive stations to the West (PYAD, PYAT, PYLO, PYPC, PYPU, PYTB). PYLS can be considered as a non directive station.

5. GROUND MOTION SIMULATIONS OF THE M_w=4.5 EVENT FROM THE M_w=3.6 EVENT: A VALIDATION TEST

5.1. How to take into account directivity effect?

In a first step, we aim to reproduce ground motions generated by the 2006 earthquake (M_w=4.5) by using the 2007 earthquake (M_w=3.6) as an empirical Green's function. In order to well reproduce observed ground motions, this led us to investigate how the directivity effect of a target event can be taken into account in our simulation method.

Among the four necessary input parameters, we considered as fixed parameters the moment magnitude of the target earthquake M_w, the moment magnitude m_w and the corner frequency f_c of the small earthquake taken as EGF (Table 3). Their values were determined in §4.2. The last needed input parameter is the ratio C between the static stress drops of the two events. Stress drop ratio parameter C can also be expressed as a function of corner frequency F_c of the target earthquake (Eq. 6):

$$C = \left(\frac{M_0}{m_0}\right)\left(\frac{F_c}{f_c}\right)^3 \quad (6)$$

Using the duration of the rupture process of the 2006 earthquake determined in §4.3, which corresponds to a value of corner frequency F_c = 1.2 Hz, we obtained a stress drop ratio C = 1.07. However, if we set as input parameter this value for all stations, we are not able to account for the directivity effect of target event. We thus introduced a new input parameter C_a which is a function of T_a the apparent rupture duration at a given station (Eq. 7):

$$C_a = \left(\frac{T_r}{T_a}\right)^3 .C \quad (7)$$

For each station the input parameter C_a was adjusted depending on the location of the station with respect to the directivity of the rupture. To be in accordance with an integer value of corner frequency ratio N, only discrete values of C_a can be used. Therefore we run simulations for which C_a parameter is set at two different values: C_a' = 2.79 (N = 2) for directive stations and C_a' = 0.83 (N = 3) for anti-directive stations (Table 4). This implies that we simulated an

earthquake with apparent rupture durations of T_a = 0.61 s for directive stations and T_a = 0.91 s for anti-directive stations.

5.2. Simulation results and comparison with data

Using the parameters given in Tables 3 and 4, we simulated at 11 stations the three-component accelerograms of 500 different earthquakes of magnitude M_w=4.5 by using the 2007 earthquake (M_w=3.6) as EGF. Examples of synthetic accelerograms are shown on Fig. 7 for four stations on the East-West component together with the EGF and the observed records. The corresponding amplitudes of the Fourier displacement spectra are presented on Fig. 8. The fit between synthetics and observed records is good in a large frequency band. Note that for frequencies lower than 0.1 Hz, the signal of the small event is dominated by noise and cannot be taken into account for the simulations.

Simulation results are also analyzed in terms of elastic acceleration response spectra, which describe the maximum response of a Single Degree of Freedom system to particular input motion as a function of natural period and damping ratio of the system. From synthetic accelerograms, for each station and each component we computed response spectra with 5% damping. Median spectral accelerations and 16th and 84th percentiles (which correspond to $\pm\sigma$, one standard deviation for a logarithmic representation), are computed to characterize ground motion variability produced by our simulations. The comparison between observed and simulated acceleration response spectra (Fig. 9) shows that ground motions observed during the 2006 earthquake (M_w=4.5) are well reproduced by our simulations. It is noticeable that the adjustment of a different input parameter C_a' for directive and for anti-directive stations was necessary to provide ground motion amplitudes consistent with effects due to directivity of the rupture. A simulation without taking into account the directivity effect would have led to a clear underestimation of ground motions for the eastern stations or an overestimation for the western stations (Fig. 10). Good reproduction of ground motion amplitudes is also true for stations on sediments affected by amplifications due to local site-effects. Indeed, the empirical Green's function simulation methods have the great advantage of incorporating wave-propagation and site effects which are information contained in the small earthquake recordings used as EGF.

These observations are also confirmed by the comparison between Peak Ground Acceleration (PGA) values recorded during the 2006 earthquake and those obtained from

simulations (Fig. 11). We obtained generally a very good fit between our simulations and the real data. It is clear that the directivity effect has a strong influence on the PGA values, as mentioned by other authors for small earthquakes (Boatwright 2007). In this application, directivity has an influence on the PGA as large as site effects. The combined effects of directivity and site can be observed on PYAT and PYLU stations which are located at the same epicentral distance. PYAT station is located on a rock site and is anti-directive whereas PYLU station is located on sediments and is directive. Its PGA value is five times larger than the one recorded at PYAT station. Our simulations reproduced generally quite well these effects, even so the directivity is only approximately taken into account, due to the discrete values imposed to the directivity factor C_a' by the constraint to keep N as integer.

6. GROUND MOTION SIMULATIONS OF AN M_w=6.1 EARTHQUAKE FROM THE M_w=3.6 EVENT

6.1. A case of blind simulation

In this part of the study, we aim to generate the ground motion recordings that could be generated by a magnitude M_w=6.1 earthquake, equivalent to the 1660 historical event. We decided to use only the 2007 earthquake (M_w=3.6) as empirical Green's function, because it is not affected by directivity effect. If the 2006 event (M_w=4.5) was chosen as EGF, it would be first necessary to compensate for directivity effect; otherwise the target event would reproduce this effect which is not suitable in a blind simulation. We will discuss later the possibility of taking into account a directivity effect in the target event.

Moment magnitude M_w of the target event, moment magnitude m_w and corner frequency f_c of the small earthquake used as EGF are fixed input parameters. However, in that case of blind simulation, the static stress drop ratio input parameter C is difficult to define as we have no a priori constraints on the static stress drop of the M_w=6.1 target event. Thus, we decided to run different simulations for which the stress drop ratio parameter C is set at different values between 0.38 and 3.43 (consistent with N integer condition). This range of C values corresponds to rupture durations between 3.6 and 7.6 seconds for the target event, which are reasonable values for such an earthquake (Table 5). Note that we tested stress drop

ratio values lower than 1.0, assuming no particular dependence of stress drop with seismic moment (e.g.: Ide & Beroza 2001; Allman & Shearer 2009), even if the question of a stress drop scaling with magnitude still remains in discussion.

For each value of C, we produced a set of 500 different synthetic accelerograms that could realistically be generated at specific stations by an M_w=6.1 earthquake. As seven different values of C are tested, we obtained a total of 3500 simulations for each station and each component. Fig. 12a shows the influence of the stress drop ratio parameter C on ground motion amplitudes: spectral acceleration levels increase with increasing C values. As nothing is known about the possible stress drop value of the target event, we decided to keep the overall acceleration distribution including the uncertainty on the stress drop ratio parameter. In order to characterize ground motion variability, we computed for each period a median value of spectral acceleration and 84^{th} -16^{th} percentiles that correspond to sigma value (Fig. 12b).

6.2. Simulation results

Fig. 13 shows ground motion levels, in terms of spectral accelerations and PGA, obtained from our simulations. The highest spectral accelerations and PGA values are obtained at station PYLO (on rock) located in the city of Lourdes, for which median PGA value is equal to 172 cm/s². For the 84^{th} percentile, a value of 347 cm/s² for PGA is reached at this station. Note that this station has an epicentral distance of only 9 km, which is theoretically at the border of application of EGF simulation methods (Irikura & Kamae 1994). We also have estimation of ground motions at stations located in the largest cities of the region. For station PYTB (on sediments) located in the city of Tarbes, at an epicentral distance of 23 km, we obtained a median PGA value of 54 cm/s². We can see that this station is affected by ground motion amplifications due to local site-effects, notably a peak of spectral accelerations at a period of about 0.4 seconds. For the city of Pau, located at an epicentral distance of about 43 km, we obtained respectively for the stations PYPC (on rock) and PYPU (on sediments) median PGA values of 20 cm/s² and 24 cm/s². In spite of different soil conditions, median PGA values are almost the same for both stations. Nevertheless, these stations present different shapes of response spectra. Station PYPU has specific ground motion amplifications at about 0.8 seconds of period. The comparison between PYAT station (on rock) and PYLU station (on sediments), located at the same source-to-site distance, shows that PYLU has

spectral accelerations and PGA values two times larger than those obtained at PYAT. We can also remark that the station on rock PYAD, which is affected by a topographic effect, exhibits unexpected high spectral accelerations and PGA values for an epicentral distance of 35 km. Indeed, it has already been noted by Drouet *et al.* (2007) that the PYAD station amplifies the high frequency content of ground motion.

In recent seismic hazard assessment studies, the acceleration levels expected for this region of the Pyrenees differ significantly from one study to another. Dubos *et al*. (2004) extrapolated PGA values obtained at PYLO for different magnitudes after attenuation correction. They estimated a maximum PGA of 100 cm/s² ± 20 cm/s² at Lourdes (on rock) for horizontal motion if a magnitude 6 earthquake were to occur 10 km away from the city. In a study of Marin *et al.* (2004), a probabilistic seismic hazard assessment has been performed for the metropolitan France and they obtained a maximum horizontal PGA around 67 cm/s² for 475-year return period (corresponding to probability of exceedance of 10% in 50 years). In a probabilistic seismic hazard assessment for the Pyrenean region using both French and Spanish data, Secanell *et al.* (2008) proposed higher values with a median PGA that reached a maximal value between 150 and 200 cm/s² for a 475-year return period. The estimations given by Dubos *et al.* (2004) and Secanell *et al.* (2008) from different kind of approaches, are in agreement with the results obtained in our study for the simulation of a magnitude M_w=6.1 earthquake at the station PYLO, whereas the study of Marin *et al.* (2004) gives a value two times lower.

6.3. Comparison with Ground Motion Prediction Equations (GMPEs)

Simulation results can be compared with different empirical ground motion prediction equations (GMPEs) to have a rough idea of the similarities and differences obtained. As the low seismic activity in France does not allow developing a specific GMPE, we have to use GMPEs based on data coming from other regions of the world. Over the years, a large number of GMPEs have been proposed (Douglas 2003) and one of difficulties is to select a GMPE that could be appropriate for an application to the Pyrenean region. In the study of Drouet *et al.* (2007), eight published GMPEs adapted for shallow crustal events were tested for their applicability to Pyrenean earthquakes by using the method of Scherbaum *et al.* (2004). Among the studied empirical models, they found that the GMPE developed by Lussou *et al.* (2001) from Japanese K-net data is the best ranked GMPE (quality class B) for an application

to Pyrenean earthquakes, whereas the others over-predict the observed ground motion records. The GMPEs of Berge-Thierry *et al.* (2003) and Ambraseys *et al.* (1996), which are usually used in seismic hazard studies in France, are respectively ranked as "acceptable" (class C) and "unacceptable" (class D). However, as noticed by the authors, we must keep in mind that the GMPEs were evaluated by applying the method to low magnitude Pyrenean earthquakes ($M_w \leq 4.0$).

We finally decided to compare our simulation results with the GMPEs of Lussou *et al.* (2001), Berge-Thierry *et al.* (2003) and Ambraseys *et al.* (2005) (Table 6). The latter are derived for estimation of PGA and pseudo-spectral accelerations (with 5% damping). All these GMPEs include soil class as explanatory variable, with a site classification based on the shear velocity averages over the upper 30 m (V_{S30}). Ambraseys *et al.* (2005) also incorporate style-of-faulting as explanatory variable. Each GMPE use different magnitude and distance definitions, thus modifications must be considered to account for these disparities. The GMPE of Ambraseys *et al.* (2005) uses directly moment magnitude M_w, whereas the GMPEs of Lussou *et al.* (2001) and Berge-Thierry *et al.* (2003) use respectively Japanese Meterological Agency magnitude M_J and surface-waves magnitude M_S. However, for a value of moment magnitude M_w of about 6.0, it is found that M_J, M_S and M_w are close (Heaton *et al.* 1986). For source-to-site distance definition, Ambraseys *et al.* (2005) uses the Joyner & Boore (1981) distance which is the distance to the surface projection of the fault. In our study, the fault dimension of the target earthquake is unknown, so the recommended approximation is to use instead epicentral distance.

Fig. 14 shows the comparison between PGA values obtained from our simulations and those predicted by the selected GMPEs for an M_w=6.1 earthquake. For each station median and 84^{th}-16^{th} percentile values of PGA computed from overall PGA distribution including an uncertainty on the stress drop ratio parameter C are compared as a function of source-to-site distance with PGA levels predicted by the GMPEs. For the comparison with the GMPEs of Lussou *et al.* (2001) and Berge-Thierry *et al.* (2003), both the North-South and the East-West components are shown. For the comparison with Ambraseys *et al.* (2005) we show the larger value of PGA from the two horizontal components. The empirical equations used are those corresponding to rock site condition, whereas for simulation results both stations on rock and on sediments are represented. When we superimpose median and 84^{th}-16^{th} percentile values of PGA obtained from simulations on those predicted by the GMPEs, we see that the standard deviation of simulations is lower or equivalent to the standard deviations of GMPEs. Note that a detailed study of the value of this standard deviation can be found in Beauval *et al.* (2009)

using that same method but another database. Globally, GMPEs of Lussou *et al.* (2001) and Ambraseys *et al.* (2005) are in good agreement with simulation results, whereas the GMPE of Berge-Thierry *et al.* (2003) is slightly higher. For distance higher than 60 km, all GMPEs supply PGA values higher than those obtained from simulations. As our simulations are based on recordings of a small magnitude event (M_w=3.6), the latter observation can be explained by a decay rate of ground motions with distance dependant on the magnitude, leading to ground motions from small events that attenuate faster with distance than those generated from large events (e.g.: Ambraseys *et al.* 2005, Bragato & Slejko 2005, Cotton *et al.* 2008).

7. COMPARISON BETWEEN SIMULATION RESULTS AND MACROSEISMIC INTENSITIES OF THE 1660 EARTHQUAKE

We have obtained on 11 points a quantification of the ground motions that could realistically be generated by an M_w=6.1 earthquake. Is there now a way to compare these results with macroseismic intensities of the 1660 historical event (Fig. 15)?

Over the years, many studies have been conducted to establish correlation equations that relate instrumental ground motion parameters to observed intensity information (e.g.: Murphy & O'Brien 1977; Trifunac & Brady 1975; Ambraseys 1974, for the oldest ones). These ground motion intensity conversion equations (GMICEs) are empirically derived through regression analysis of database for which we have both ground motion records and intensity observations as close as possible to each recording station. GMICEs are mostly developed for rapid damage assessment, like shake map application. However, the availability of such empirical relationships enables also to use historical information and to estimate possible ground motion parameter ranges for past earthquakes. In our case, GMICEs provide us with the opportunity to make a direct link between our ground motion simulations and the intensities of the 1660 historical earthquake. To transform the PGA and PGV values we obtained from simulations into intensity values, we proposed to use three different PGA-Intensity and PGV-Intensity empirical relationships recently developed by Wald *et al.* (1999), Atkinson & Kaka (2007) and Tselentis & Danciu (2008). The datasets used to derive these GMICEs and their intensity ranges of validity are indicated in Table 7. Wald *et al.* (1999) empirical relationships are those usually used to produce shake maps in California. These

PGA-Intensity and PGV-Intensity correlation equations are derived by using data from eight large Californian earthquakes. Atkinson & Kaka (2007) relationships were developed from small to moderate earthquakes both felt and recorded in Central United States region. This database was supplemented with data from larger events that occurred in California. The equations defined by Atkinson & Kaka (2007) take into account the influence of magnitude and distance, which is not the case for the equations of Wald et al. (1999). The empirical relationships developed by Tselentis & Danciu (2008) are based on data recorded in Greece and include effects of magnitude, distance and local soil conditions. Note that intensity values cannot be estimated from these equations with a precision better than one intensity unit.

Using these three GMICEs, we computed an intensity level for each station from median values of PGA obtained from simulations. On Fig. 16, the intensity ranges obtained from ground motion simulations are compared with macroseismic intensities of the 1660 historical earthquake assessed from interpretation of historical documents (SisFrance, BRGM *et al.* 2004). We note that two different intensity scales are used: macroseismic intensities of the 1660 event are expressed in the MSK scale (Medvedev *et al.* 1964), whereas the results obtained from empirical relationships are expressed in the Modified Mercalli Intensity scale (Wood & Neumann 1931; see Musson *et al.* (2009) for a review of a large number of intensity scales). However, as shown by Barosh (1969), the two scales are essentially similar over the whole range of values. Fig. 16 clearly shows that intensity values obtained from PGA of simulations are too small compared with macroseismic intensities of the 1660 earthquake. For example, at a distance of about 10 kilometres we obtained intensity values equal to VI or VI-VII from simulations, whereas at the same distance for the 1660 earthquake the macroseismic intensity is estimated to VIII, corresponding to major destructions. Indeed, it has been reported on historical documents that this earthquake induced strong damages, notably in the cities of Lourdes and Bagnères-de-Bigorre. On the whole, there is a difference of at least two intensity units between macroseismic intensities assessed for the 1660 earthquake and intensity levels predicted by empirical relationships from simulation results.

The same work was done from 84th percentile values of PGA and intensity levels reached a maximal value of VII at a distance of 10 km. Moreover, even if the three different GMICEs used here are developed for different regions of the world, the results are in good agreement between themselves. Similar results are obtained with the PGV, which is sometimes recognized as a better indicator of the destructive potential of ground motions than PGA (e.g.: Wald *et al.* 1999; Boatwright *et al.* 2001; Kaka & Atkinson 2004).

8. DISCUSSION: WAS THE 1660 EARTHQUAKE LARGER THAN M_w=6.1?

In the previous section, we have observed that intensity levels corresponding to our ground motion simulations of an M_w=6.1 earthquake are clearly lower than macroseismic intensities of the 1660 historical earthquake. This result led us to discuss the origin of this discrepancy, in particular to question whether the 1660 event is larger than an M_w=6.1 earthquake. In order to make a critical analysis of this hypothesis, the following points have to be discussed:

- Macroseismic information

As stated previously, collecting historical information to establish macroseismic maps is not an easy task. In the case of the 1660 event, the macroseismic epicentre appears rather well defined (within 10 km). However, if the 1660 event was affected by a strong directivity effect, the macroseismic epicentre may be shifted from several kilometres with respect to the real epicentre (e.g.: Grandin *et al.* 2007, for the 1755 great Lisbon earthquake). Thus the location of the 1660 event may be somewhat different from that of the two small events.

Moreover, no information is known about the depth of the 1660 event. The distance between isoseists is informative of this depth, thus depth may theoretically be retrieved from the macroseismic maps if an attenuation model is available (Levret *et al.* 1994). Although the depth is not given in the historical catalogs for the 1660 event, its isoseists are clearly those of a superficial event, similarly to most of the Pyrenean events. Levret *et al.* (1994) also show that 70% of the focii of French historical events are in the depth range 2.5-12.5 km. It is thus realistic to ascribe to the 1660 event the same depth as that of the small event used as EGF.

- Magnitude of the 1660 event

The macroseismic magnitude of the 1660 event (*Ml*=6.1±0.4; Levret *et al.* 1996) was obtained by using the Levret *et al.* (1994) relationship between local magnitude, intensity and focal distance. This empirical relationship was established from 73 French earthquakes for which macroseismic data and instrumental magnitude are both available.

Uncertainties are cumulated at each processing step of historical data analysis. Error in epicentral intensity and/or in focal depth can thus strongly bias the estimation of

macroseismic magnitude. Given that focal depth is unknown for the 1660 event, it should have a consequence on its magnitude estimation: the magnitude would be underestimated if the focal depth is underestimated.

A more critical point is that the magnitude-intensity relationship is established with only two events with $Ml \geq 6$, thus it is poorly constrained for large magnitudes. Moreover, a single relationship is established for the whole French metropolitan territory, but significant regional variations in attenuation have been observed (Drouet *et al.* 2008). The strongest attenuation in the Pyrenees may results in an underestimation of the magnitudes from the standard intensity-magnitude relationship.

The magnitude determined by Levret *et al.* (1996) is a local magnitude *Ml*, whereas we use a moment magnitude M_w for simulating the ground motions. It is well known that these two magnitude scales do not always give the same values. For the Pyrenees, Drouet *et al.* (2005) found on instrumental earthquakes a difference of about 0.5 between these two magnitudes. Note that it was the case also for the two small events we used in this paper (the November 17th, 2006 event (Ml=5.0, M_w=4.5) and the November 15th, 2007 event (Ml=4.1, M_w=3.6)). If we follow this rule to convert *Ml* to M_w, it would predict a moment magnitude of about M_w=5.6 for the 1660 event. If we had taken this value in our simulations, the ground motion estimation would have been even smaller and then the adequation with macroseismic data would be even worse. However, we must keep in mind that the study of Drouet *et al.* (2005) is based on small to moderate earthquakes and we do not know if it can be extrapolated to larger earthquakes.

- Shortcomings of the method

If we assume that the magnitude M_w=6.1 ascribed to the 1660 earthquake is correct (Cara *et al.* 2008), some shortcomings of the EGF simulation method should be pointed out to explain differences between simulation results and intensity data of the 1660 event.

The EGF method doesn't account for nonlinear soil behavior. This point is certainly not so crucial in our study because the levels of acceleration found are rather low and should not engender non linear effects.

This method provides site-specific simulations, which is a great advantage to take into account particular effects. Nevertheless the punctual intensity data of the 1660 event were not obtained at the same points, which make tough the comparison between simulation results and punctual intensity data of the 1660 event.

This simulation method is based on a point-source representation of the fault and thus doesn't allow precisely taking into account a specific directivity effect of the rupture process. Nevertheless, for a given stress drop ratio input parameter *C*, a large number of ESTFs with different shapes and durations is randomly generated and they can implicitly account for various directivity effects. Additionally, we decided to run different simulations for which *C* is set at seven different values corresponding to rupture durations from 3.6 to 7.6 seconds for the target event. As we have no indication about the rupture of the 1660 event, it can still led us to wonder whether the ground motions variability produced by our simulations is large enough.

- Complex relationship between macroseismic intensities and instrumental ground motion parameters

The last point that has to be investigated is the use of GMICEs to transcribe simulation results into intensity values. In our case, in spite of the opportunity that offers this kind of relationships, we must keep in mind that macroseismic intensity represents, on a qualitative and discrete scale, a complex function between ground motions, damage levels and human perception of shaking. Response of the structures and human sensitivity are frequency-dependent, whereas each ground motion parameter represents different characteristics and frequency content of the seismogram (Souriau 2006). It is thus particularly difficult to define a correlation equation between instrumental ground motion parameters and macroseismic intensity. Differences between simulation results and intensity data of the 1660 event can also be explained by the unknown fragility of damaged constructions before the earthquake. So, we concluded that GMICEs should be used cautiously to predict intensity levels from simulation results. We thus have to temper the interpretation of results, especially when comparing with macroseismic intensities of an historical event, such as 1660 earthquake.

9. CONCLUSION

Using the opportunity of two moderate earthquakes very well recorded by an accelerometric network in the Pyrenees, we simulated seismograms of a larger event similar to the 1660

historical earthquake that caused many damages to constructions. We first validated the approach by simulating an M_w=4.5 event using an M_w=3.6 event as empirical Green's functions. Data analysis revealed a clear directivity effect of the rupture process of the M_w=4.5 event which, once taken into account, leads to a very good agreement between observations and simulations. We found that this directivity effect has a similar influence on ground motions than stress drop variation. We proposed a simple way to take into account directivity effects in our simulations together with stress drop. We observed on this example that directivity effect has a stronger influence on ground motion levels than site effects.

Using the M_w=3.6 event, which does not exhibit directivity in its rupture, we then simulated the 1660 historical event. This simulation allowed us to generate realistic seismograms and to estimate the PGA in the main cities where destructions have been reported. They are consistent with the predictions of empirical ground motion equations (GMPEs). We then converted our simulation results in macroseismic intensity using three different empirical ground motion intensity conversion equations (GMICEs). We found that our values were always lower than the macroseismic intensities collected. This inconsistency led us to suspect the validity of the conversion from macroseismic intensities to magnitude, or to suggest that the 1660 event had a magnitude larger than M_w=6.1.

The development of high dynamic networks in the world enables us to use now more accurately the records of small events to simulate larger ones. This approach is promising for simulating the ground motion of a future earthquake, which is a realistic hypothesis in the Pyrenean region. At the same time, the drawing up of macroseismic intensity maps, in particular for large events, together with the computation of reliable regional attenuation models appear of major importance to be able to make the link between historical and instrumental seismicity.

ACKNOWLEDGMENTS

We thank all the persons in charge of the seismological and accelerometric networks in the French Pyrenees and particularly Mathieu Sylvander and Marie Calvet from the Obervatoire Midi-Pyrenéees and Pascal Dominique from BRGM. We also thank the RAP (Réseau Accélérométrique Permanent Français) team that enables everyone to dispose of high quality

data. We thank David Baumont from Institut de Radioprotection et de Sureté Nucléaire and Michel Cara (IPGS) for fruitful discussions. Financial support has been provided by the French Ministry of Environment through the Groupement d'interêt scientifique GIS RAP and the French Ministry of Enseignement Supérieur et Recherche for the grant thesis.

REFERENCES

Aki, K., 1967. Scaling law of seismic spectrum, *J. geophys. Res.,* **72**, 1217-1231.

Alasset, P-J. & Meghraoui, M., 2005. Active faulting in the western Pyrénées (France): paleoseismic evidence for late Holocene ruptures, *Tectonophysics*, **409**, 39-54.

Allmann, B.P. & Shearer, P.M., 2009. Global variations of stress drop for moderate to large earthquakes, *J. geophys. Res.*, **114**, B01310, doi: 10.1029/2008JB005821.

Ambraseys, N., 1974. The correlation of intensity with ground motions, *Proc. of the 14th Conf. of the European Seismological Commission*, Trieste, Italy.

Ambraseys, N., Simpson, K.A. & Bommer, J.J., 1996. Prediction of horizontal response spectra in Europe, *Int. J. Earthq. Eng. Struct. Dyn.*, **25**, 371-400.

Ambraseys, N.N., Douglas, J., Sarma, S.K. & Smit, P.M., 2005. Equations for the estimation of strong ground motions from shallow crustal earthquakes using data from Europe and the Middle-East: horizontal peak ground acceleration and spectral acceleration, *Bull. seism. Soc. Am.*, **3**, 1-53, doi:10.1007/s10518-005-0183-0.

Atkinson, G.M. & Kaka, S.I., 2007. Relationships between felt intensity and instrumental ground motion in the central United States and California, *Bull. seism. Soc. Am.,* **97**, 497-510.

Barosh, P.K., 1969. Use of seismic intensity data to predict the effects of earthquakes and underground nuclear explosions in various geological settings, *US Geol. Survey Bull*, **1279**, Washington D.C., 93 pp.

Beauval, C., Honoré, L. & Courboulex, F., 2009. Ground-motion variability and implementation of a probabilistic-deterministic hazard method, *Bull. seism. Soc. Am*., **99**, 2992-3002, doi:10.1785/0120080183.

Beeler, N.M., Wong, T.F. & Hickman, S.H., 2003. On the expected relationships between apparent stress, static stress drop, effective shear fracture energy and seismic efficiency, *Bull. seism. Soc. Am*., **93**, 1381-1389.

Berge-Thierry, C., Cotton, F., Scotti, O., Griot-Pommera, D.A. & Fukushima, Y., 2003. New empirical response spectral attenuation laws for moderate European earthquakes, *J. Earthq. Eng.*, **7**, 193-222.

Bernard, P., Czitrom, G., Dubié, J-Y., Godefroy, P., Lambert, J. & Levret-Albaret, A., 1997. Les tremblements de Terre en France, Lambert J. (Editor), *Editions BRGM*, Orléans, 196 pp.

Boatwrigth, J., Thywissen, K. & Seekins, L., 2001. Correlation of ground motion and intensity for the 17 January 1994 Northridge, California, earthquake, *Bull. seism. Soc. Am*., **91**, 739-752.

Boatwright, J., 2007. The persistence of directivity in small earthquakes, *Bull. Seism. Soc. Am.*, **97**, 1850-1861.

Bragato, L. & Slejko, D., 2005. Empirical ground-motion attenuation relations for the eastern Alps in the magnitude range 2.5-6.3, *Bull. seism. Soc. Am*., **95**, 252-276.

BRGM-IRSN-EDF, 2004. Histoire et caractéristiques des séismes ressentis en France métropolitaine et sur ses abords, SisFrance catalog, available at: http://www.sisfrance.net/ (last accessed September 2010)

Brune, J.N., 1970. Tectonic stress and the spectra of seismic shear waves from earthquakes, *J. geophys. Res*., **75**, 4997-5009.

Cara, M., Alasset, P.-J. & Sira, C., 2008. Magnitude of historical earthquakes, from macroseismic data to seismic waveform modelling : application to the Pyrenees and a 1905 earthquake in the Alps, *Historical Seismology*, **2**, 369-384, doi: 10.1007/978-1-4020-8222-1_18.

Choukroune, P., 1992. Tectonic evolution of the Pyrenees, *Annu. Rev. Earth planet. Sci.,* **20**, 143-158.

Cotton, F., Pousse, G., Bonilla, F. & Scherbaum, F., 2008. On the discrepancy of recent European ground-motion observations and predictions from empirical models: analysis of Kik-net accelerometric data and point-sources stochastic simulations, *Bull. seism. Soc. Am*., **98**, 2244-2261, doi:10.1785/0120060084.

Courboulex, F., Converset, J., Balestra, J. & Delouis, B., 2010. Ground-Motion Simulations of the 2004 Mw 6.4 Les Saintes, Guadeloupe, Earthquake Using Ten Smaller Events, *Bull. seism. Soc. Am*., **100**, 116-130, doi :10.1785/0120080372.

Douglas, J., 2003. Earthquake ground motion estimation using strong-motion records: a review of equations for the estimation of peak ground acceleration and response spectral ordinates, *Earth-Science Reviews*, **61**, 43-104.

Drouet, S., Souriau, A. & Cotton, F., 2005. Attenuation, seismic moments, and site effects for weak-motion events: application to the Pyrenees, *Bull. seism. Soc. Am.*, **95**, 1731-1748, doi:10.1785/0120040105.

Drouet, S., Scherbaum, F., Cotton, F. and Souriau, A., 2007. Selection and ranking of ground motion models for seismic hazard analysis in the Pyrenees, *J. Seism.*, **11**, 87-100, doi:10.1007/s10950-006-9039-6.

Dubos, N., Sylvander, M., Souriau, A., Ponsolles, C., Chevrot, S., Fels, J-F. & Benahmed, S., 2004. Analysis of the 2002 May earthquake sequence in the central Pyrenees, consequences for the evaluation of the seismic risk at Lourdes, France, *Geophys. J. Int.*, **156**, 527-540, doi:10.1111/j.1365-246X.2004.02091.x.

Gagnepain, J., Modiano, T., Cisternas, A., Ruegg, J.C., Vadell, M., Hatzfeld, D. & Mezcua, J., 1980. Sismicité de la région d'Arette (Pyrénées Atlantiques) et mécanismes au foyer, *Ann. Geophys.*, **36**, 499-508.

Gagnepain-Beyneix, J., Haessler, H. & Modiano, T., 1982. The Pyrenean earthquake of February 29 1980, an example of complex faulting, *Tectonophysics*, **85**, 273-290.

Gallart, J., Banda, E. & Daignières, M., 1981. Crustal structure of the Paleozoic Axial Zone of the Pyrenees and the transition to the North Pyrenean Zone, *Ann. Géophys.*, **37**, 457-480.

Grandin, R., Borges, J.F., Bezzegoud, M., Caldeira, B. & Carrilho, F., 2007. Simulations of strong ground motion in SW Iberia for the 1969 February 28 (Ms=8.0) and the 1755 November 1 (M~8.5) earthquakes – II. Strong ground motion simulations, *Geophys. J. Int.*, **171**, 807-822.

Hartzell, S.H., 1978. Earthquake aftershocks as Green's functions, *Geophys. Res. Lett*., **5**, 1-4.

Heaton, T.H., Tajima, F. & Mori, A.W., 1986. Estimating ground motions using recorded accelerograms, *Surv. Geophys.*, **8**, 25-83.

Hirn, A., Daignières, M., Gallart J. & Vadell, M., 1980. Explosion seismic sounding of throws and dips in the continental Moho, *Geophys. Res. Lett.*, **7**, 263-266.

Ide, S. & Beroza, G.C., 2001. Does apparent stress vary with earthquake size?, *Geophys. Res. Lett.,* **28**, 3349-3352.

Irikura, K. & Kamae, K., 1994. Estimation of strong ground motion in broad-frequency band based on a seismic source scaling model and an empirical Green's function technique, *Annali di Geofisica*, **XXXVII**, 1721-1743.

Joyner, W.B. & Boore, D.M., 1981. Peak horizontal acceleration and velocity from strong-motion records including records from the 1979 Imperial Valley, California, earthquake, *Bull. seism. Soc. Am.*, **71**, 2011-1038.

Joyner, W.B. & Boore, D.M., 1986. On simulating large earthquakes by Green's function addition of smaller earthquakes, in Earthquake Source Mechanics, Vol.37, *Maurice Ewing Series 6*, Das, S., Boatwright, J. & Scholtz, C.H. (Editors), American Geophysical Union, Washington, D.C., 269-274.

Kaka, S.I. & Atkinson, G.M., 2004. Relationships between instrumental ground-motion parameters and modified Mercalli intensity in eastern North America, *Bull. seism. Soc. Am.*, **94**, 1728-1736.

Kanamori, H. & Anderson, D.L., 1975. Theorical basis of some empirical relations in seismology. *Bull. seism. Soc. Am.*, **65**, 1073-1095.

Kanamori, H. & Rivera, L., 2004. Static and dynamic scaling relations for earthquakes and their implications for rupture speed and stress drop, *Bull. seism. Soc. Am.*, **94**, 314-319.

Kohrs-Sansorny, C., Courboulex, F., Bour, M. & Deschamps, A., 2005. A two-stage method for ground-motion simulation using stochastic summation of small earthquakes, *Bull. seism. Soc. Am.*, **95**, 1387-1400.

Lambert, J. & Levret-Albaret, A., 1996. Mille ans de séismes en France, *Ouest Editions*, Nantes, 78pp.

Levret, A., Backe, J.C. & Cushing, M., 1994. Atlas of macroseismic maps for French earthquakes with their principal characteristics, *Natural Hazards*, **10**, 19-46.

Levret, A., Cushing, M. & Peyridieu, G., 1996. Recherche des caractéristiques de séismes historiques en France. Atlas de 140 cartes macrosismiques, IPSN, Paris, France (2 vol.).

Lussou, P., Fukushima, Y., Bard, P.Y. & Cotton, F., 2001. Seismic design regulation codes: contribution of Knet data to site effect evaluation, *J. Earthq. Eng.*, **5**, 13-33.

Marin, S., Avouac, J-P, Nicolas, M. & Schlupp, A., 2004. A probabilistic approach to seismic hazard in metropolitan France, *Bull. seism. Soc. Am.*, **94**, 2137-2163.

Medvedev, S., Sponheuer, W. & Karnik, V., 1964. Neue seismische Skala Intensity scale of earthquakes, 7.Tagung der Europäischen Seismologischen Kommission vom 24.9. bis 30.9.1962. In: Jena, Veröff. Institut für Bodendynamik und Erdbebenforschung in Jena, Vol.77. Deutsche Akademie der Wissenschaften zu Berlin, 69-76pp.

Murphy, J.R. & O'Brien, L.J., 1977. The correlation of peak ground acceleration amplitude with seismic intensity and other physical parameters, *Bull. seism. Soc. Am.*, **67**, 877-915.

Musson, R.M.W., Grünthal, G. & Stucchi, M., 2009. The comparison of macroseismic intensity scales, *J. Seism.,* **14**, 413-428, doi:10.1007/s10950-009-9172-0.

Nocquet, J.-M. & Calais, E., 2004. Geodetic measurements of crustal deformation in the Western Mediterranean and Europe, *Pure appl. Geophys.*, **161**, 661-681.

Olivet, J.L., 1996. La cinématique de la plaque Ibérique (Kinematics of the Iberian Plate), *Bull. Centres Rech. Explor.-Prod. Elf Aquitaine*, **20**, 131-195.

Ordaz, M., Arboleda, J. & Singh, S.K., 1995. A scheme of random summation of an empirical Green's function to estimate ground motions from future large earthquakes, *Bull. seism. Soc. Am.*, **85**, 1635-1647.

Pequegnat, C., Guéguen, P., Hatzfeld, D. & Langlais, M., 2008. The French Accelerometric Network (RAP) and National Data Center (RAP-NDC), *Seismol. Res. Lett.*, **79**, 79-89.

Reiter, L., 1990. *Earthquake Hazard Analysis: Issues and Insights*, Columbia University Press, New York, 254 pp.

Rigo, A., Souriau, A., Pauchet, H., Grésillaud, A., Nicolas, M., Olivera, C. & Figueras, S., 1997. The February 1996 earthquake sequence in the eastern Pyrenees: first results, *J. Seism.*, **1**, 3-14, doi:10.1023/A:1009711512921.

Rigo, A., Souriau, A., Dubos, N., Sylvander, M. & Ponsolles, C., 2005. Analysis of the seismicity in the central part of the Pyrenees (France), and tectonic implications, *J. Seism.*, **9**, 211-222.

Ruiz, M., Gallart, J., Diaz, J., Olivera, C., Pedreira, D., Lopez, C., Gonzalez-Cortina, J.M. & Pulgar, J.A., 2006. Seismic activity at the western Pyrenean edge, *Tectonophysics*, **412**, 217-235, doi:10.1016/j.tecto.2005.10.034.

Salichon, J., Kohrs-Sansorny, C., Bertrand, E. & Courboulex, F., 2010. A Mw 6.3 earthquake scenario in the city of Nice (South-East France): Ground motion simulations, *J. Seism.* in press, doi:10.1007/s10950-009-9180-0.

Scherbaum, F., Cotton, F. & Smit, P., 2004. On the use of response spectral reference data for the selection and ranking of ground-motion models for seismic hazard analysis in regions of moderate seismicity: the case of rock motion, *Bull. seism. Soc. Am.*, **94**, 1-22.

Secanell, R., Bertil, D., Martin, C., Goula, X., Susagna, T., Tapia, M., Dominique, P., Carbon, D. & Fleta, J., 2008. Probabilistic seismic hazard assessment of the Pyrenean region, *J. Seism.*, **12**, 323-341, doi:10.1007/s10950-008-9094-2.

Souriau, A. & Pauchet, H., 1998. A new synthesis of Pyrenean seismicity and its tectonic implications, *Tectonophysics*, **290**, 221-244.

Souriau, A., Sylvander, M., Rigo, A., Fels, J-F., Douchain, J-M. & Ponsolles, C., 2001. Sismotectonique des Pyrénées : principales contraintes sismologiques, *Bull. Soc. Géol. France*, **172**, 25-39.

Souriau, A., 2006. Quantifying felt events: a joint analysis of intensities, accelerations and dominant frequencies, *J. Seism.*, **10**, doi:10.1007/s10950-006-2843-1.

Sylvander, M., Souriau, A., Rigo, A., Tocheport, A., Toutain, J-P., Ponsolles, C. & Benahmed, S., 2008. The 2006 November, Ml=5.0 earthquake near Lourdes (France): new evidence for NS extension across the Pyrenees, *Geophys. J. Int.*, **175**, 649-664, doi:10.1111/j.1365-246X.2008.03911.x.

Trifunac, M.D. & Brady, A.G., 1975. On the correlation of seismic intensity with peaks of recorded ground motion, *Bull. seism. Soc. Am.*, **65**, 139-162.

Tselentis, G-A. & Danciu, L., 2008. Empirical relationships between modified mercalli intensity and engineering ground-motion parameters in Greece, *Bull. seism. Soc. Am.*, **98**, 1863-1875, doi:10.1785/0120070172.

Vogt, J., 1979. Les tremblements de terre en France, *Mem. BRGM*, **96**, Orleans, France, 220pp.

Wald, D.J., Quitoriano, V., Heaton, T.H. & Kanamori, H., 1999. Relationships between peak ground acceleration, peak ground velocity, and modified Mercalli intensity in California, *Earthq. Spectra*, **15**, 557-564.

Wennerberg, L., 1990. Stochastic summation of empirical Green's functions, *Bull. seism. Soc. Am.*, **80**, 1418-1432.

Wood, H.O. & Neumann, F., 1931. Modified Mercalli Intensity scale of 1931, *Bull. seism. Soc. Am.*, **21**, 277-283.

FIGURE LEGENDS

Figure 1. The two principal steps of the study. In Step 1 (validation test) the 2007 earthquake (M_w=3.6) is used as an empirical Green's function to reproduce ground motions generated by the 2006 earthquake (M_w=4.5). Simulation results and ground motions observed during the 2006 earthquake are directly compared. In Step 2 (blind simulation) the 2007 earthquake (M_w=3.6) is used as an empirical Green's function to produce ground motion simulations of a magnitude M_w=6.1 earthquake, equivalent to the 1660 historical event. Simulation results and intensity data of the 1660 event are indirectly compared by using empirical relationships between instrumental ground motion parameters and macroseismic intensities.

Figure 2. Instrumental seismicity for the period 1989-2009 (from Observatoire Midi-Pyrénées catalogs) and largest historical events with maximal MSK macroseismic intensity VIII and IX; NPF: North Pyrenean Fault.

Figure 3. Isoseists contour lines and intensity domains (on MSK scale, 1964) for the 1660 historical earthquake (SisFrance catalog, BRGM *et al.* 2004).

Figure 4. Epicentres (red dots) and focal mechanisms of the two selected instrumental earthquakes (Sylvander *et al.* 2008) and location of the 11 Pyrenean accelerometric stations used in this study. Stations on rock and on sediments are indicated with different colours. Black star: macroseismic epicentre of the 1660 historical earthquake, given with a location uncertainty of about 10 km (SisFrance catalog, BRGM *et al.* 2004).

Figure 5. Corner frequencies obtained at each station from displacement spectra analysis as a function of event-to-station azimuth for the November 2007 earthquake (M_w=3.6) and the November 2006 earthquake (M_w=4.5). For the first earthquake the values obtained are rather stable with azimuth, with an average value (blue line) of 3.3 Hz and a standard deviation

(dotted blue lines) of 0.3 Hz. For the second earthquake a clear dependency of the corner frequency with azimuth can be found. It can be explained by a directivity effect of the rupture process.

Figure 6. Directivity analysis of the November 2006 earthquake (M_w=4.5). Inset shows the variation of the linear correlation coefficient as a function of azimuth of rupture propagation. The best value is found for directivity towards 114°. For this selected value of directivity, the figure shows a plot of apparent source time function duration (T_a) as a function of the directivity factor Gamma (Γ).

Figure 7. Accelerograms of the observed 2006 earthquake (in black) compared with a sample of three simulations (in red) out of the 500 generated at four stations (PYPC, PYPU, PYLS and PYTB) and accelerograms of the 2007 earthquake used as EGF (in blue).

Figure 8. Fourier displacement spectra of the observed 2006 earthquake (in black) at four stations (PYPC, PYPU, PYLS and PYTB) compared with an average simulation (in red) and displacement spectra of the 2007 earthquake used as EGF (in blue).

Figure 9. Elastic response spectra in acceleration of the observed 2006 earthquake (in black) superimposed for each station on median and 84^{th}-16^{th} percentiles (in red) computed from 500 acceleration response spectra (in grey) for East component. C_a' parameter is adjusted depending on the location of the station with respect to the directivity of the rupture: C_a'=2.79 for directive stations and C_a'=0.83 for anti-directive stations.

Figure 10. Examples of simulation results for PYAT and PYLI stations (East component) when C parameter is not adjusted to account for effects due to directivity of the rupture. **(a)** When C parameter is set to 0.83, we obtain an underestimation of observed ground motions (in black) for the directive station PYLI; **(b)** When C parameter is set to 2.79, we obtain an overestimation of observed ground motions (in black) for the anti-directive station PYAT.

Figure 11. PGA values observed for the 2006 earthquake (black stars) as a function of epicentral distance compared with median PGA values and 16^{th}-84^{th} percentiles computed from 500 simulations for each station (East component). Note the influence of the directivity, which induces higher PGAs for the directive stations (in red) than for the anti-directive ones (in blue).

Figure 12. (a) Seven sets of 500 acceleration response spectra (5% damping) obtained for each stress drop ratio parameter *C* tested for the simulation of an M_w=6.1 earthquake at PYAT station (East component). Median spectral accelerations computed for each *C* value are superimposed; **(b)** Overall spectral acceleration distribution including an uncertainty on the stress drop ratio parameter *C* (in grey) and median with 84^{th}-16^{th} percentiles (in black).

Figure 13. Simulation results in terms of acceleration response spectra (in grey) and median PGA (values in red) obtained for an M_w=6.1 earthquake at each station (East component). Median and 84^{th} -16^{th} percentiles (in black) are computed from overall spectral acceleration distribution including an uncertainty on the stress drop ratio parameter *C*.

Figure 14. Peak Ground Accelerations (black and grey symbols) obtained from simulation of the M_w=6.1 earthquake at each station (both rock and soil sites) as a function of source-to-site distance: median and 84^{th}-16^{th} percentiles computed from overall PGA distribution including an uncertainty on the stress drop ratio parameter *C*. They are compared with PGA values predicted for rock site conditions by the ground motion prediction equations of **(a)** Lussou *et al.* (2001) on both horizontal components (black: East, grey: North); **(b)** Berge-Thierry *et al.* (2003) on both horizontal components (black: East, grey: North); **(c)** Ambraseys *et al.* (2005) for the larger horizontal component.

Figure 15. Macroseismic intensities (MSK scale, 1964) and isoseists for the June 21^{st}, 1660 historical earthquake. The macroseismic epicentre of the 1660 event is plotted as a black star

with a location uncertainty of about 10 km. Intensity value assigned to each point was assessed from interpretation of available historical documents where accounts of felt shaking and damage levels are reported (SisFrance catalog, BRGM *et al.* 2004).

Figure 16. Comparison between macroseismic MSK intensities of the 1660 earthquake (SisFrance, BRGM *et al.* 2004) and intensity levels (MMI scale) expected at each station from ground motion simulations of an M_w=6.1 earthquake. For each station, median values of PGA of simulations (including an uncertainty on the stress drop ratio parameter) are transcribed into intensity values (± one intensity unit) by using PGA-Intensity empirical relationships of Wald *et al.* (1999), Atkinson & Kaka (2007) and Tselentis & Danciu (2008).

TABLES

Date	Time (UTM)	*Ml*	Hypocentral location			Focal mechanism		
			Lat. (°)	Long. (°)	Depth (km)	Plane 1		
						Strike (°)	Dip (°)	Rake (°)
2006/11/17	18h19m51s	5.0	43.0282	0.0032	9.7	284	56	-84
2007/11/15	13h47m35s	4.1	43.0207	0.0022	7.8	296	30	-50

Table 1. Hypocentral locations and focal mechanism parameters (from Sylvander *et al.* 2008) of the two instrumental earthquakes used in this study.

Station name	Locality	Latitude (°)	Longitude (°)	Elevation (m)	Local site geology
PYAD	Arudy	43.098	-0.426	450	Rock
PYAS	Aspet	43.012	0.797	430	Sediment
PYAT	Arette	43.095	-0.711	340	Rock
PYBB	Bagnères-de-Bigorre	43.059	0.149	560	Rock
PYLI	St Lizier	43.002	1.136	424	Rock
PYLO	Lourdes	43.098	-0.048	410	Rock
PYLS	Luz-St-Sauveur	42.860	-0.009	770	Rock
PYLU	Luchon	42.791	0.601	630	Sediment
PYPC	Pau (castle)	43.296	-0.374	200	Rock
PYPU	Pau (university)	43.315	-0.366	208	Sediment
PYTB	Tarbes	43.226	0.049	305	Sediment

Table 2. Location and local site geology for the Pyrenean accelerometric stations used in this study. All of them belong to the French Permanent Accelerometric Network (see: http://www-rap.obs.ujf-grenoble.fr)

Date	M_w	F_c (Hz)	C
2006/11/17	4.5	1.2	1.07
2007/11/15	3.6	3.3	

Table 3. Fixed input parameters for the simulation of the 2006 earthquake (M_w=4.5) by using the 2007 earthquake (M_w=3.6) as empirical Green's function. F_c is the corner frequency and C the static stress drop ratio.

Station	Az (°)	F_a (Hz)	C_a	N	C_a'
PYLI	95	1.60	2.56	2	2.79
PYAS	96	1.54	2.29	2	2.79
PYBB	102	1.80	3.60	2	2.79
PYLU	123	1.54	2.29	2	2.79
PYLS	184	1.30	1.37	2	2.79
PYAT	272	0.96	0.55	3	0.83
PYAD	273	1.02	0.65	3	0.83
PYLO	293	1.04	0.69	3	0.83
PYPC	308	1.00	0.62	3	0.83
PYPU	311	1.00	0.62	3	0.83
PYTB	11	1.10	0.82	3	0.83

Table 4. Apparent corner frequency F_a obtained at each station from data analysis of the 2006 earthquake (see Fig. 5) and input parameters used to include directivity effect of the target event; C_a' parameter is consistent with N integer condition.

Fixed input parameters		
M_w	m_w	f_c (Hz)
6.1	3.6	3.3
Variable input parameter		
C	T_r (s)	
0.38	7.57	
0.43	7.27	
0.74	6.06	
1.02	5.45	
1.45	4.85	
2.16	4.24	
3.43	3.64	

Table 5. Input parameters for the simulation of the M_w=6.1 earthquake by using the 2007 earthquake (M_w=3.6) as EGF. Moment magnitude M_w of the target event, moment magnitude m_w and corner frequency f_c of the EGF are fixed input parameters. Static stress drop ratio C is a variable input parameter taking 7 different values in the range [0.38 3.43]. T_r are the corresponding rupture duration values.

Authors	Area and time coverage of dataset	Magnitude range of validity	Distance range of validity (km)	Horizontal component definition
Lussou *et al.* (2001)	Japan 1996-1998	$3.5 \leq M_J \leq 6.3$	$10 \leq R_{hypo} \leq 200$	Not specified
Berge-Thierry *et al.* (2003)	Europe (83%) California (17%) 1952-1997	$4.0 \leq M_S \leq 7.9$	$4 \leq R_{hypo} \leq 330$	Both horizontal components
Ambraseys *et al.* (2005)	Europe and Middle East 1973-2003	$M_w \geq 5.0$	$R_{JB} < 100$	Larger horizontal component

Table 6. Ground motion prediction equations (GMPEs) used for the comparison with simulation results. Given are magnitude and distance definition and their associated range of validity. M_J is Japanese Meteorological Agency magnitude, M_S is surface-waves magnitude, M_w is moment magnitude, R_{hypo} is hypocentral distance and R_{JB} is Joyner & Boore (1981) distance.

Authors	Dataset	Intensity range of validity	Horizontal component definition
Tselentis & Danciu (2008)	Greece (1973-1999) $4 \leq M_w \leq 6.9$	IV ≤ MMI ≤ VIII	Both horizontal components
Wald *et al.* (1999)	California (1971-1994) $5.8 \leq M_w \leq 7.3$	V ≤ MMI ≤ VIII	Geometric mean
Atkinson & Kaka (2007)	Central United States (2000-2005) $1.8 \leq M_w \leq 4.6$ + California (2000-2004) $3.5 \leq M_w \leq 7.1$	II ≤ MMI ≤ IX	Both horizontal components

Table 7. Datasets used to derive ground motion intensity conversion equations (GMICEs) with their intensity range of validity and the horizontal component definition. M_w is moment magnitude and MMI is Modified Mercalli Intensity.

FIGURES

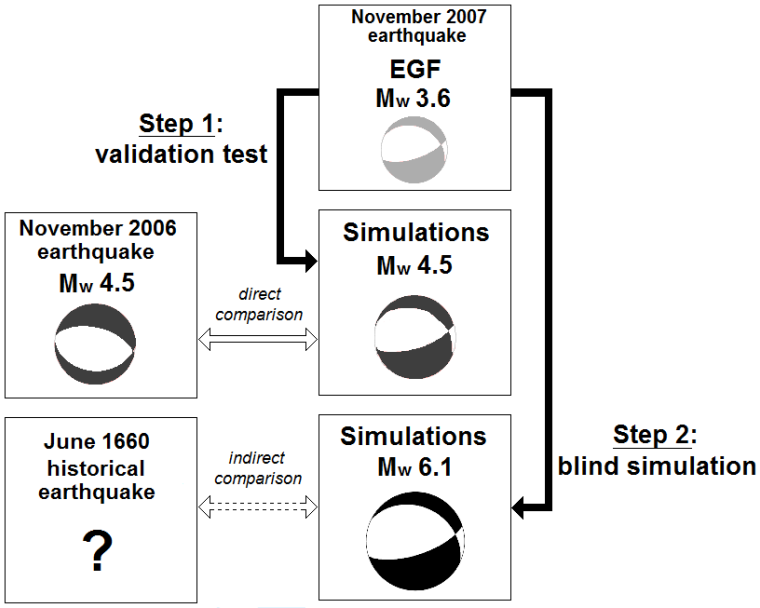

Figure 1

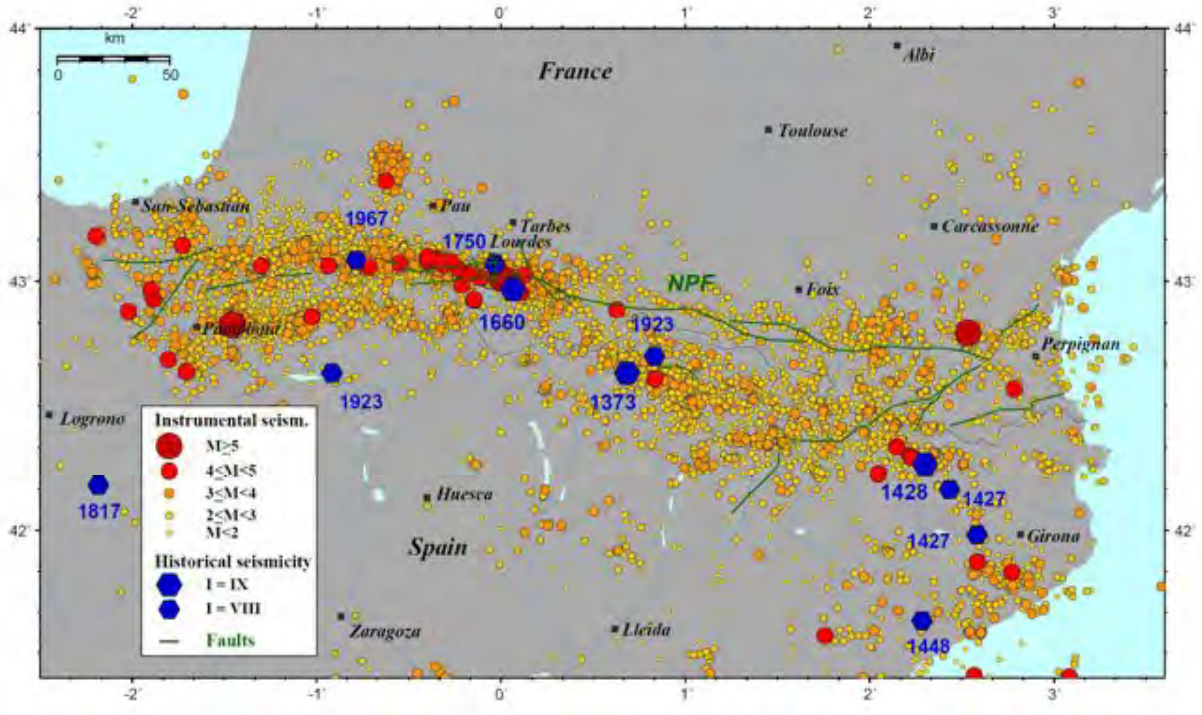

Figure 2

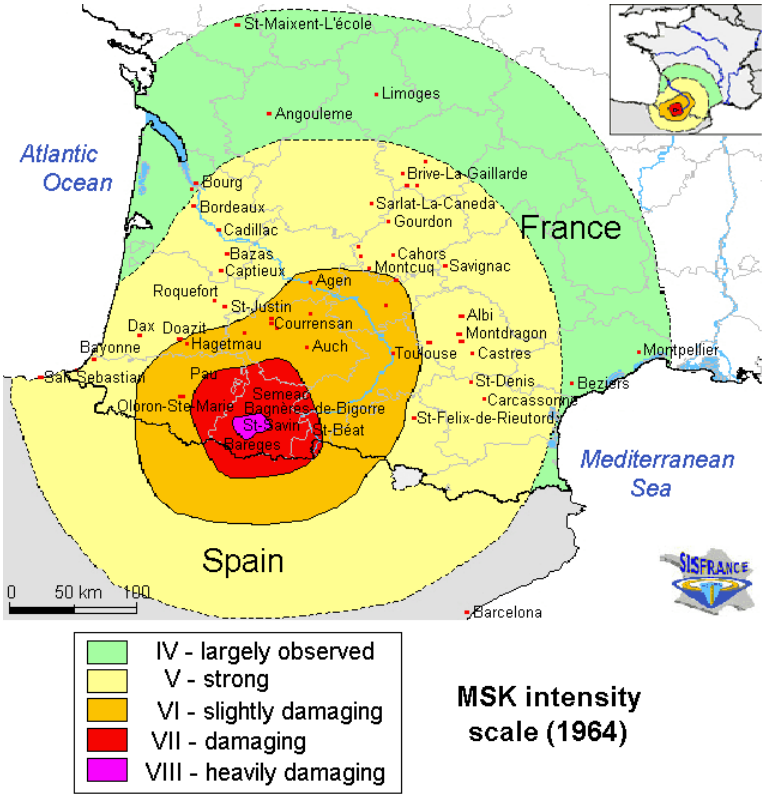

1211
1212
1213 **Figure 3**
1214
1215
1216

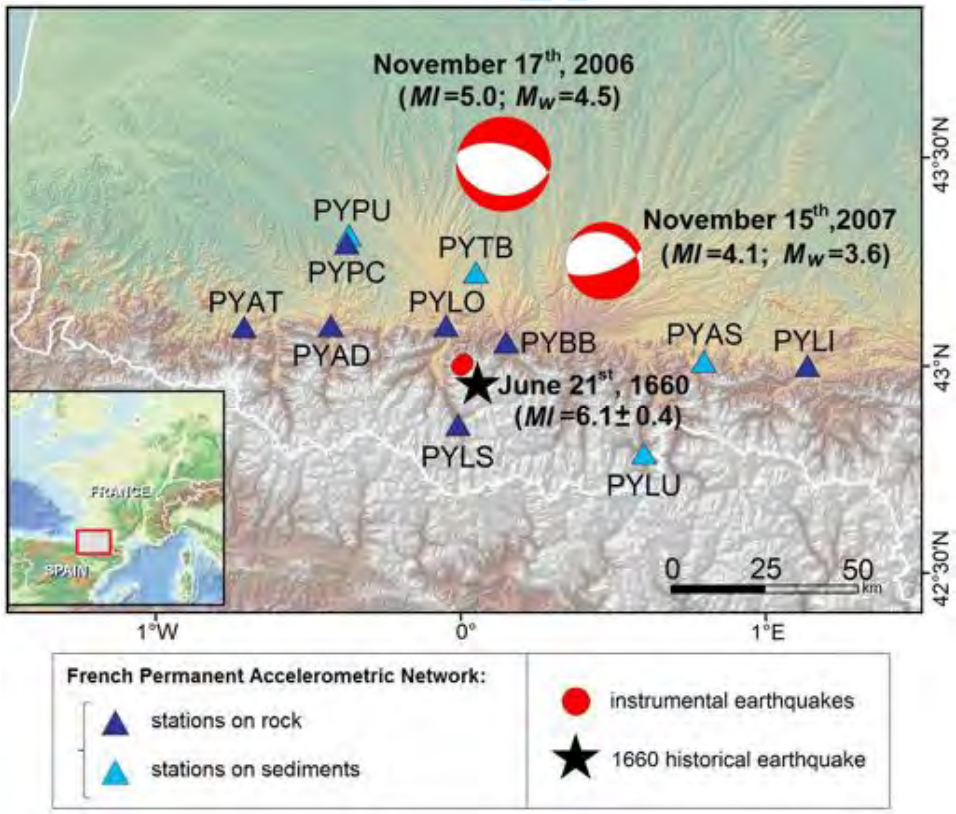

1217
1218
1219 **Figure 4**

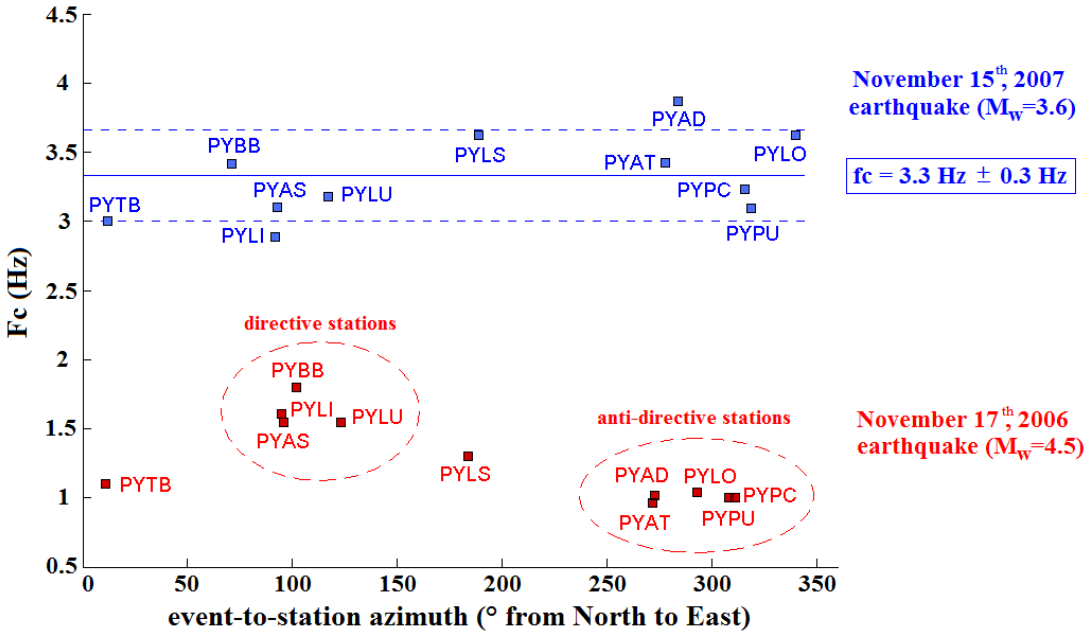

Figure 5

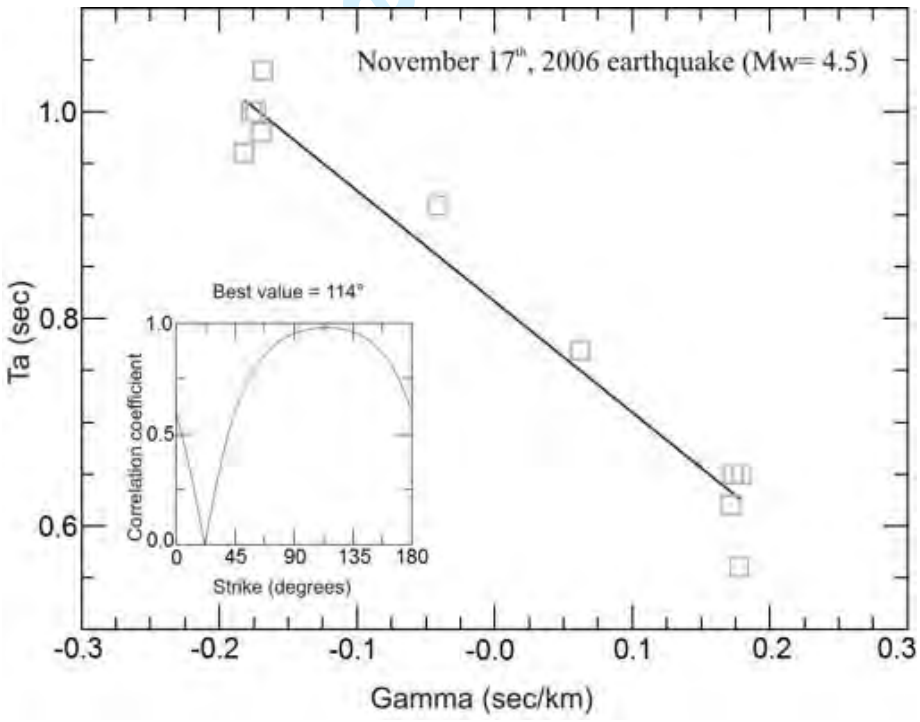

Figure 6

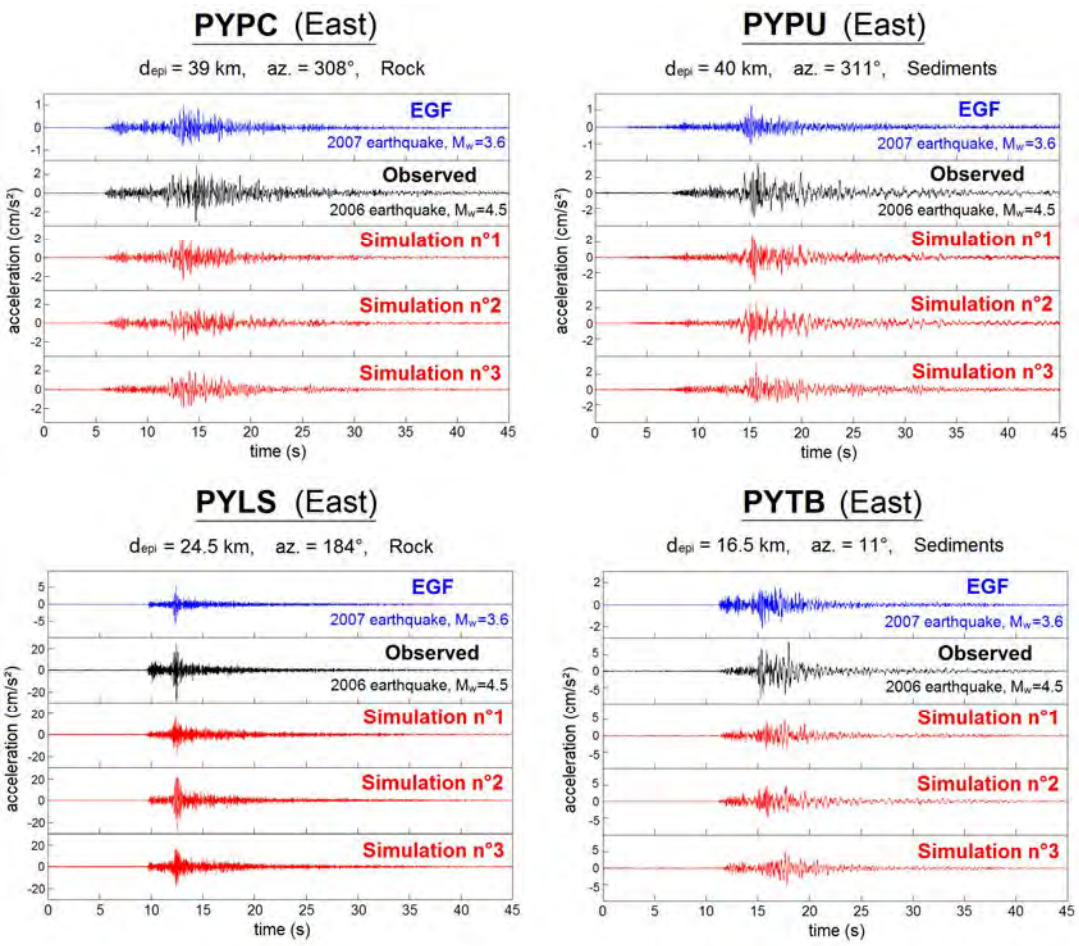

Figure 7

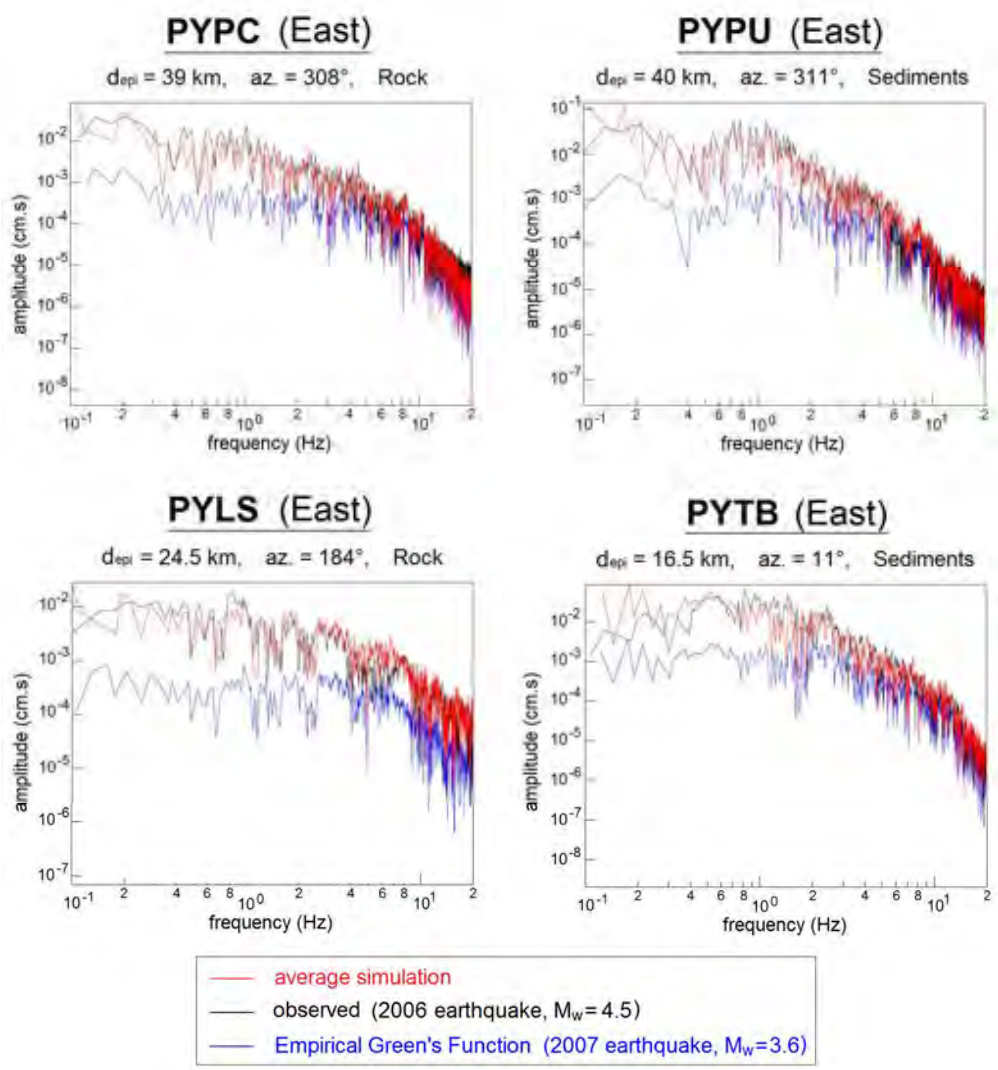
PYPC (East)
depi = 39 km, az. = 308°, Rock
PYPU (East)
depi = 40 km, az. = 311°, Sediments
PYLS (East)
depi = 24.5 km, az. = 184°, Rock
PYTB (East)
depi = 16.5 km, az. = 11°, Sediments
amplitude (cm.s)
frequency (Hz)
average simulation
observed (2006 earthquake, Mw = 4.5)
Empirical Green's Function (2007 earthquake, Mw=3.6)

Figure 8

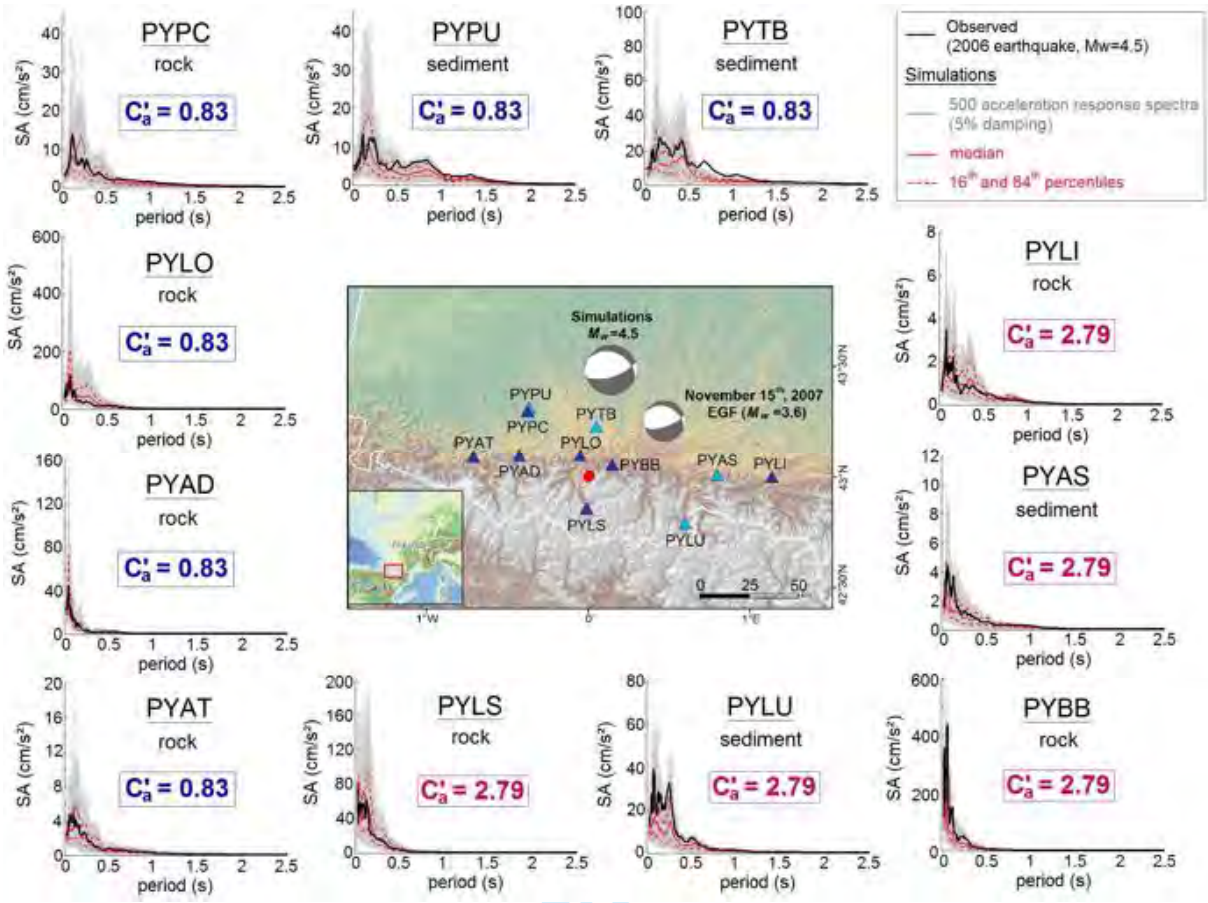

Figure 9

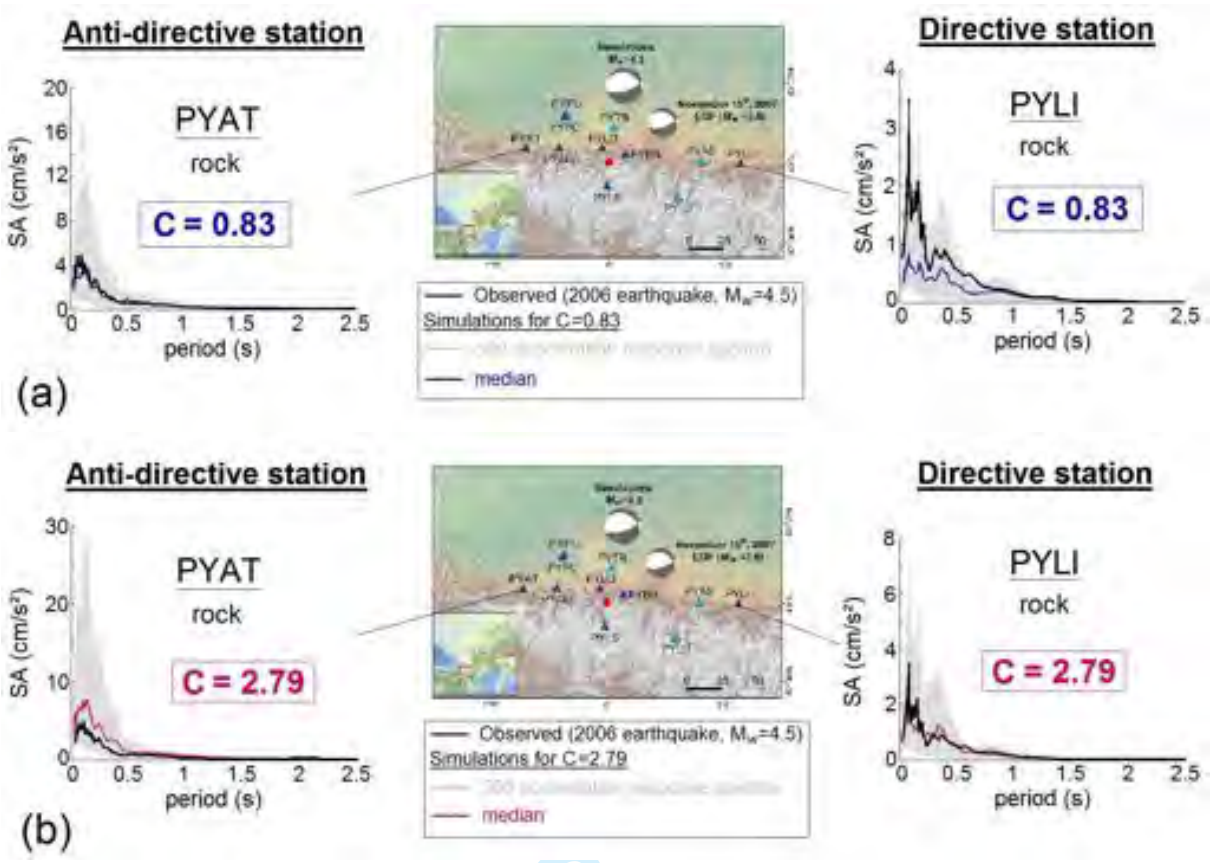

Figure 10

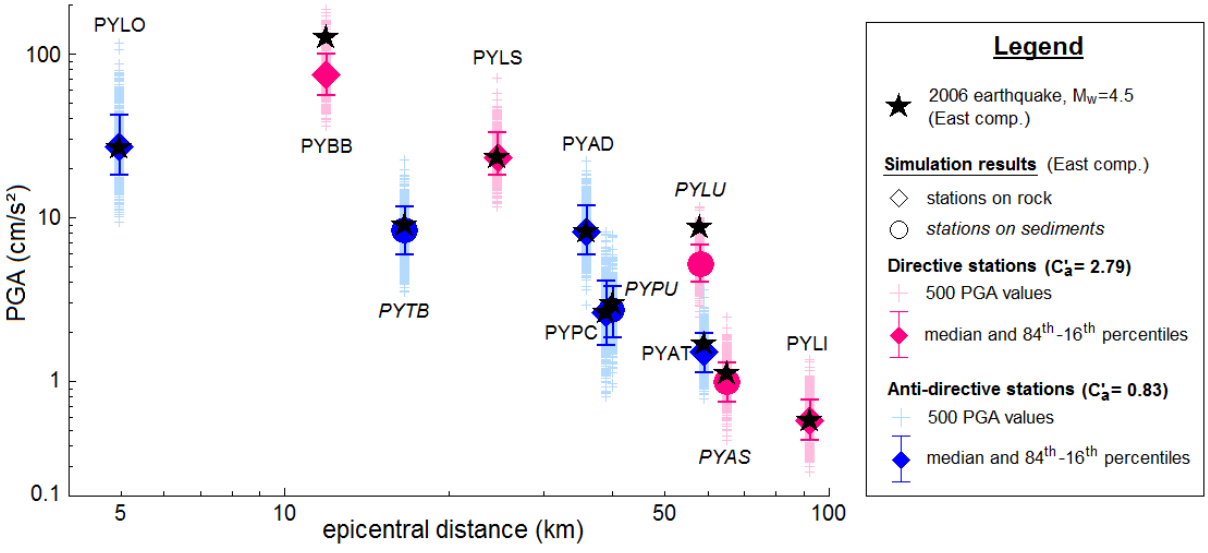

Figure 11

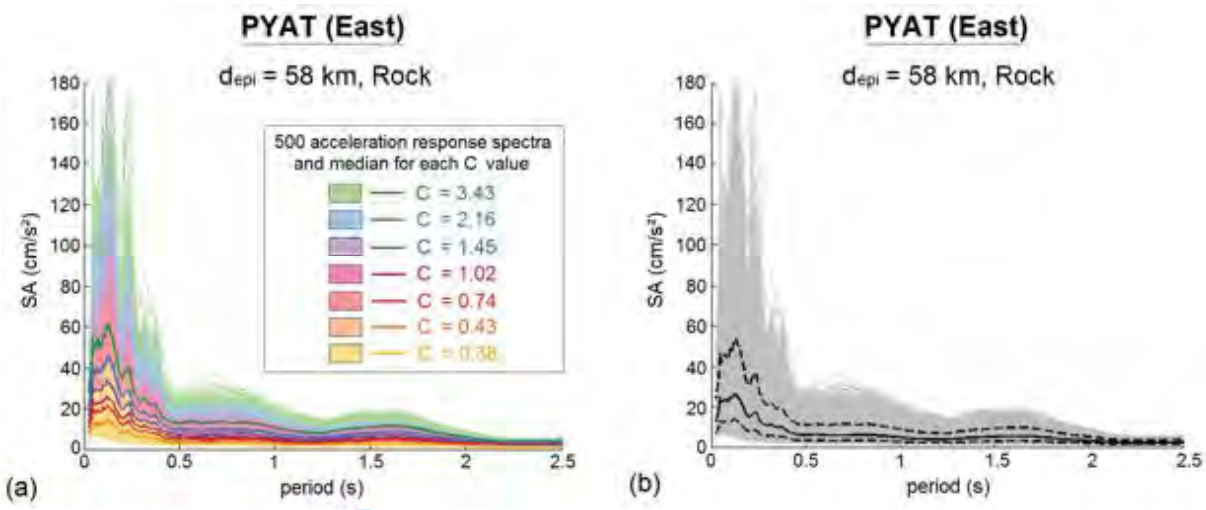

Figure 12

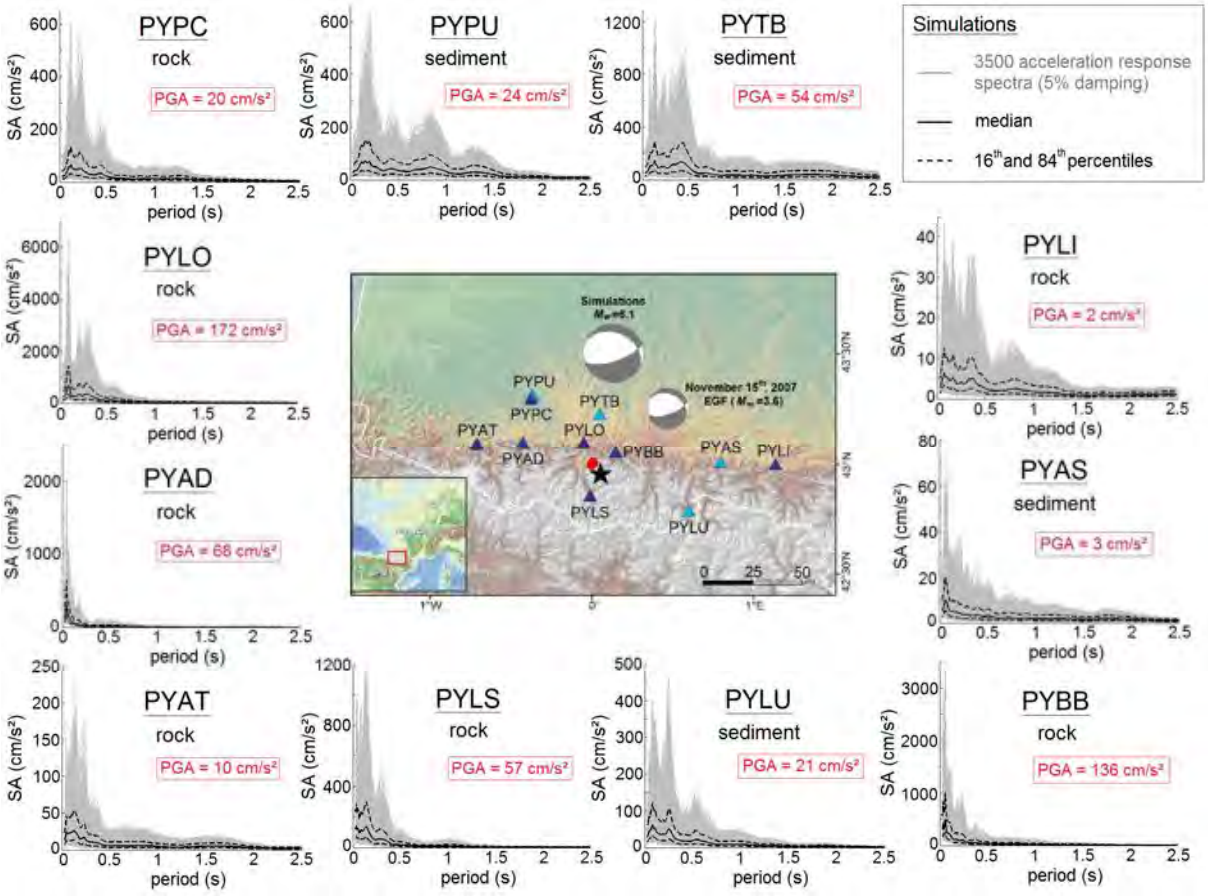

Figure 13

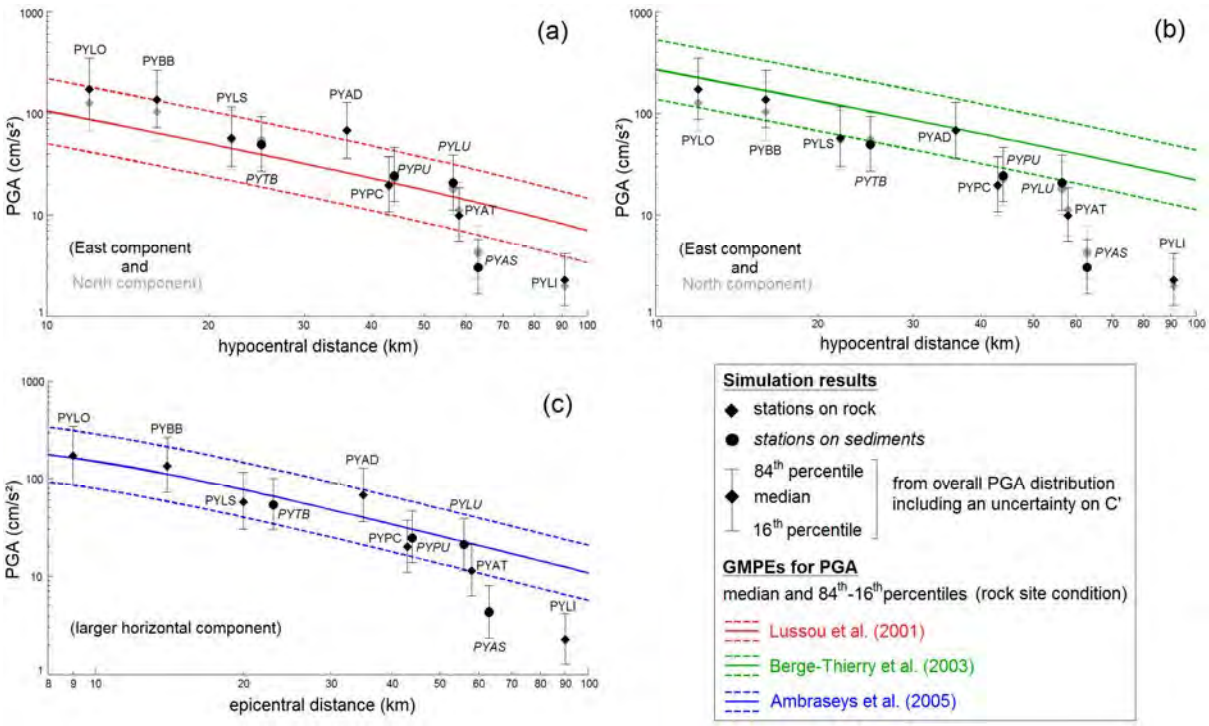

1274
1275
1276 **Figure 14**
1277
1278
1279

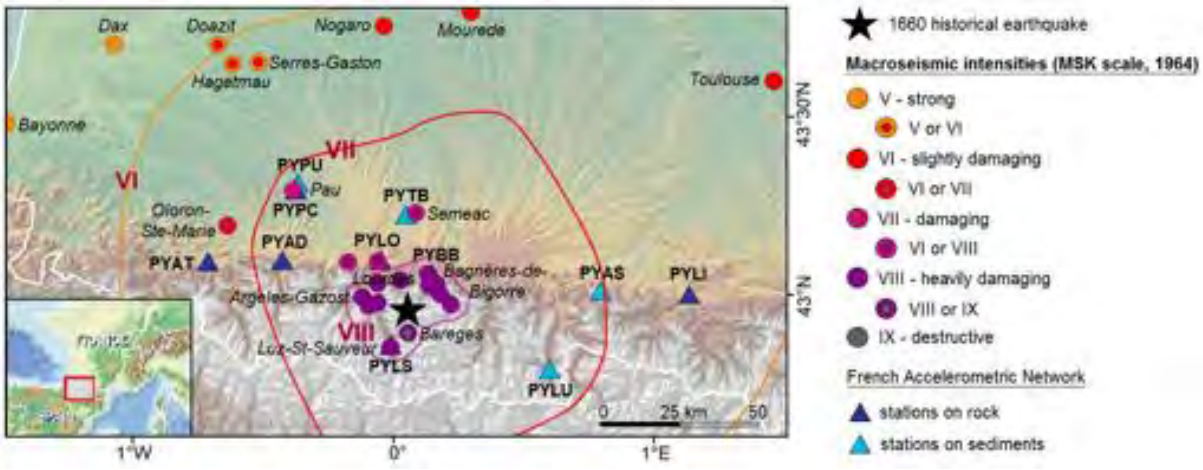

1280
1281
1282 **Figure 15**
1283
1284
1285

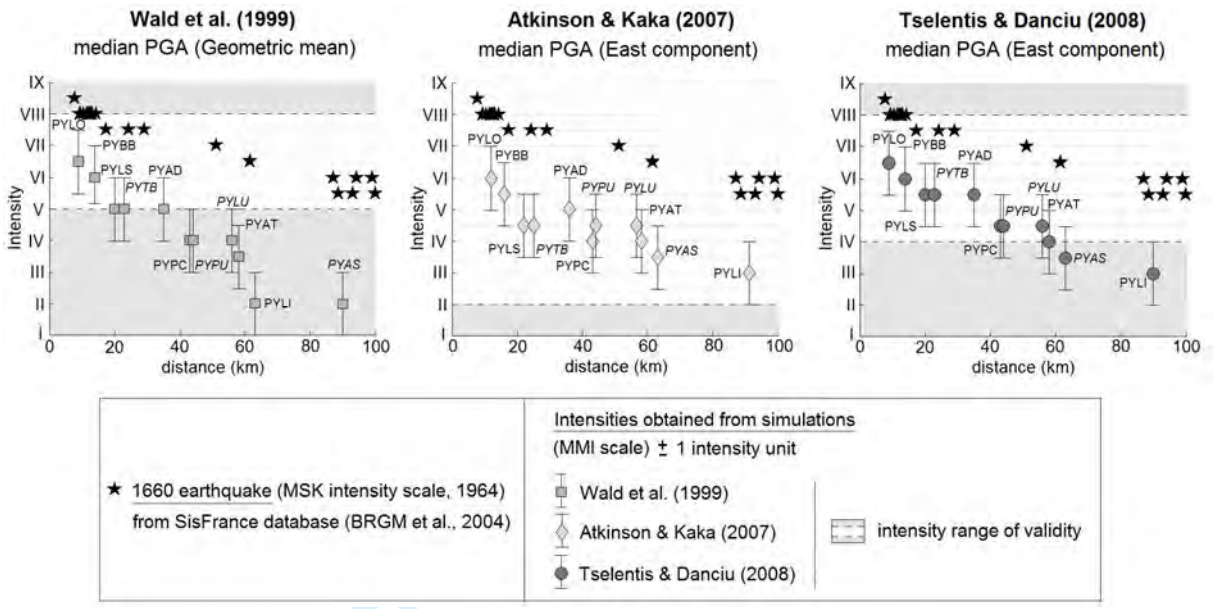

1286
1287
1288 **Figure 16**